BOUNDARY-LAYER PROFILES OF PARTICULATE MATTER SIZE DISTRIBUTIONS USING A BALLOON-BORNE LIGHTWEIGHT AEROSOL SPECTROMETER

by

ANNICK MARIE MALETTO

B.Sc., Concordia University, 2000

A THESIS SUBMITTED IN PARTIAL FULFILMENT OF
THE REQUIREMENTS FOR THE DEGREE OF

MASTER OF SCIENCE

in

THE FACULTY OF GRADUATE STUDIES

(Atmospheric Science Programme)

We accept this thesis as conforming
to the required standard

THE UNIVERSITY OF BRITISH COLUMBIA

October 2002

Department of Earth & Ocean Sciences

The University of British Columbia
Vancouver, Canada

Date October 10, 2002

Abstract

A novel method in making cost-effective size-segregated vertical profiles of PM_{10} up to one kilometre above the earth's surface is evaluated. The performance of a commercial miniature particle mass spectrometer, the GRIMM Particle Dust Monitor 1.108, is tested for sensitivity to varying wind speed in a wind tunnel with quasi-controlled environment. The instrument's ability to take accurate measurements is further tested against two calibrated instruments. The results show that, with calibration, the instrument is suitable for obtaining vertical profiles. The instrument was also deployed on a 5 m^3 tethered balloon at two sites in the Lower Fraser Valley, British Columbia during the summer of 2001. The results of the field study provide a complete diurnal evolution of PM_{10} in the vertical, a day time and night time comparison of mass distributions with altitude, evaluation of an elevated pollution layer, and validation with Lidar.

TABLE OF CONTENTS

List of Tables

List of Figures

Acknowledgements

I would like to thank my committee for providing excellent guidance throughout my work and always being available. Special thanks goes to my supervisor, Ian McKendry, for all his help and incredible patience. I would also like to thank Chris Gorry and Paul Bovis for their help in collecting the data and, specifically, for agreeing to stay out entire nights. Mention also goes to Pacific 2001 and their collaboration on this research and especially to Kevin Strawbridge for providing the Lidar data. This work and my program was supported by the Natural Sciences and Engineering Research Council of Canada.

Chapter I: Introduction

The stimulus for this research was the almost complete lack of direct observations evident in the literature of the changing size distribution of particulate matter (PM) with elevation in the planetary boundary layer (PBL). PM_{10} (particulate matter with an aerodynamic diameter of 10 μm or less) research is relatively recent and most data result from surface monitoring networks with a coarse spatial resolution (McKendry, 2000). Most studies have focused on source apportionment but some research is now concentrating on the development of dispersion models (Neu *et* al, 1994; Kleeman *et al.*, 1999). These models are largely based on previous air quality models developed for gaseous pollutants, more specifically, ozone. The modifications basically involve changing ozone sources and sinks to those of PM_{10}. However, an important difference between ozone and PM_{10}, which is presently ignored in air quality models, is their physical structure.

Ozone is a gas hence its structure is homogeneous where as PM_{10} is composed of particles of various sizes. Ozone and PM_{10} may therefore behave differently when airborne. Ozone is well mixed in the daytime boundary layer hence its vertical distribution is quasi-homogeneous (Pisano *et al.*, 1997). PM_{10} may not have a homogeneous vertical distribution. It is possible that its vertical distribution, with respect to particle size, varies with height and, consequently, its vertical distribution varies with respect to total concentration.

A heterogeneous vertical structure could have implications for the residence time of PM_{10} and, as a result, its dispersion. If larger particles remain close to the surface, then they should have a lower residence time as they are more likely to collide with obstructions and be deposited.

Smaller particles are likely to have a longer residence time and thus be dispersed greater distances. This may be especially important in coastal cities with complex terrain. Ozone research has indicated that the local meteorology of such locations tends to create elevated pollution layers that can be re-circulated to the surface producing severe pollution episodes (Ulrickson and Mass, 1990; McElroy and Smith, 1993; Lu and Turco, 1995; Steyn, 1996; McKendry and Lundgren, 2000). Elevated pollution layers of particulate matter have also been observed, however, the particle size distribution for these layers is unknown (Wakimoto and McElroy, 1986; Hoff et al., 1996; Raj et al. 1997; Ferrare *et al.*, 1998; Hamonou et al., 1999). It is likely that, if they have a significantly greater residence time, smaller particles are responsible for elevated particulate matter layers and are therefore more likely to be re-circulated. In all, it may be more reasonable to model PM_{10} in parts rather than as a single pollutant.

The vertical distribution of PM_{10}, with respect to particle size and total concentration, has not been observed with the exception of the Stettler and Hoyningen-Huene (1996) study which included only one measurement point above the surface. This limited amount of research may largely be a consequence of instrument inadequacy as existing instruments for PM_{10} measurement are either not portable or cannot take real-time measurements. The relatively recent emergence of miniature particle spectrometers (e.g. the GRIMM Particle Dust Monitor 1.108) has raised the possibility that such instruments could be deployed on balloons to provide size-segregated profiles of PM in the PBL. There is some doubt, however, concerning the GRIMM's ability to obtain accurate airborne measurements under varying wind conditions and rapidly changing concentrations.

This research has two main objectives:

(1) to determine if a GRIMM Particle Dust Monitor 1.108 is suitable for obtaining airborne measurements via deployment on a tethered balloon and, if so,

(2) to obtain size-segregated vertical profiles of PM_{10} in order to observe its vertical distribution with respect to particle size and total concentration.

Laboratory tests to investigate the GRIMM's sensitivity to varying wind speeds were conducted at the University of British Columbia (Geography Department). Calibration of the GRIMM was conducted at two separate sites during June, July, and August 2001. A description of the methodology is presented in Chapter 3. Results for wind sensitivity tests and calibration are provided in Chapter 4.

Chapter 5 describes two case studies, the first from Pitt Meadows (July 2001) and the second from Langley Township (August 2001), that resulted from the summer field campaign. The Langley Township study was part of the Pacific 2001 Field Study – a large inter-agency collaborative study focusing of PM_{10} and ozone in the Lower Fraser Valley.

The next chapter reviews air pollution meteorology in coastal regions with complex terrain and current PM_{10} knowledge. Health effects, sources and sinks, spatial and temporal variations, and expected vertical distribution of PM_{10} are presented.

Chapter II: Current State of Knowledge on PM_{10}

2.1. Introduction

The effect of PM_{10} on human morbidity and mortality has become a major concern over the past decade. Consequently, research on the pollutant is in its early stages. Adequate emission abatement strategies largely depend on the development and validation of physical/chemical models. Model development and validation requires extensive observations. Unfortunately, extensive air pollution data sets are difficult to obtain and expensive. Acquisition of such data sets is usually possible with large co-operative studies of which there are few with respect to PM_{10}.

The California Regional $PM_{10}/PM_{2.5}$ Air Quality Study (CRPAQS) is currently conducting intensive research in the Los Angeles Basin with respect to surface-level measurements (Solomon and Magliano, 1999). The Pacific 2001 Field Study was a large inter-agency collaborative study for PM_{10} and ozone in the Lower Fraser Valley of British Columbia. The objectives include the acquisition of a substantial three-dimensional data set for PM_{10}. These studies may significantly improve the current state of knowledge for PM_{10} and, subsequently, lead to the development of valid dispersion models.

The current state of knowledge on PM_{10} is limited. This chapter provides a review of PM_{10} research. A brief review of air pollution meteorology in coastal regions with complex terrain is also presented to help in evaluating potential PM_{10} behaviour.

2.2. Health Effects

Atmospheric particulate matter is a pollutant composed of liquid and solid particles that vary in size and chemical composition (McKendry and Lundgren, 2000). Particulate matter has long been considered, as a result of epidemiological studies, to significantly impact human morbidity and mortality (Berico *et al.*, 1997; Vedal, 1997; Gunter, 1999). In the past two decades, however, such studies have indicated that hazardous particulate matter is primarily composed of solid particulates with a diameter of less than 10 μm (PM_{10}) (Gunter, 1999).

PM_{10} is deemed harmful because it is 'inhalable', that is, it can penetrate the respiratory system beyond the nasal cavity and be deposited deep into the lungs (Berico *et al.*, 1997; Gunter, 1999; McKendry and Lundgren, 2000). Very high short term exposure can result in pulmonary edema while moderate long term exposure can reduce lung efficiency and subsequently lead to cardiopulmonary disease (Berico *et al.*, 1997; Gunter, 1999). In addition, PM_{10} can carry polycyclic aromatic hydrocarbons (PAH) - a known carcinogen (Zheng *et al.*, 2000).

There are four levels of penetration into the respiratory system by atmospheric particulates: (1) nasal cavity, (2) trachea and bronchi, (3) bronchiole, and (4) alveoli (see Figure 2.1). The level of penetration, and subsequent health effects, is dependent on particle size (see Table 2.1).

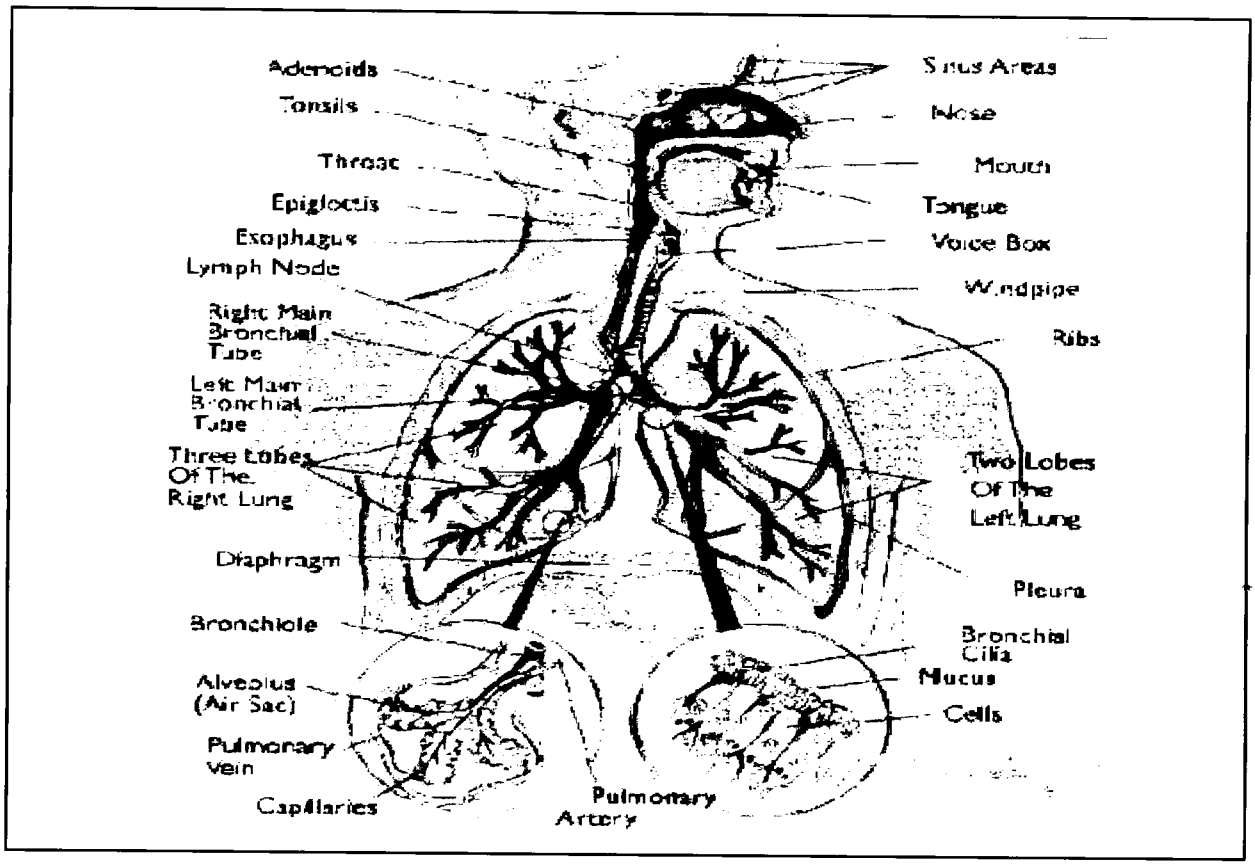

Figure 2.1: Human respiratory system (American Lung Association, 2002).

The rising concern regarding the impacts of PM_{10} has resulted in the implementation of safety standards for PM_{10} concentrations (see Table 2.2) (Gunter, 1999). These guidelines require cities to monitor PM_{10} concentrations and, if these exceed the guidelines, to develop emission abatement strategies (Gunter, 1999). The EPA has more recently adopted guidelines for $PM_{2.5}$ as these fine particulates are now believed to be the most harmful component of PM_{10} (Zheng *et al.*, 2000). It should be noted, however, that there has been some recent debate concerning the ability of epidemiological studies to properly isolate the effects of PM_{10} on human health.

Level 1: PM	Penetration into the nasal cavity does not have serious consequences. It can, however, cause some nasal congestion or irritation as well as watery eyes especially in persons suffering from allergies. The relatively mild effects explain why non-inhalable particles are not considered a health risk.
Level 2: PM_{10}	Penetration to the trachea/bronchi can irritate the bronchial walls thus making the bronchi more susceptible to infections (bronchitis). This level of penetration is particularly harmful to persons suffering from chronic bronchitis and allergies.
Level 3: PM_5	Penetration to the bronchiole may also increase the chance of infections and it may cause light respiratory difficulties. More notable, however, is the effect of level 3 penetration on persons suffering from asthma. Asthma is itself a form of 'overreaction' to airborne particles and allergens. High PM_{10} episodes are well correlated with increases in asthma-related deaths and hospitalisations.
Level 4: $PM_{2.5}$	Particles penetrating the respiratory system up to level 3 become trapped in mucus and are eventually removed by cilia (small 'hairs') that move the mucus up and out of the body. Particles penetrating to the 4^{th} level, however, cannot be removed this way. Alveoli do not have cilia so particles become trapped. The body, however, senses the particles as 'foreign' objects and thus attempts to remove them with white blood cells, that is, it attempts to remove the particles in the same manner that it would remove an infection. The white blood cell (macrophages) literally engulph the particles in the alveoli. In doing so, the white blood cells leave scar tissue on the wall of the alveoli. Scar tissue is thicker and tougher than normal tissue hence the overall result is the toughening of the alveoli that can lead to serious health effects. Alveoli are responsible for gas exchange in the lung, that is, uptaking of CO_2 from the pulmonary artery and delivering O_2 to the pulmonary vein. Scar tissue reduces the efficiency of this process making it more difficult to deliver O_2 to the heart. This, in turn, strains the heart as it must provide more blood in order to achieve the same total amount of O_2. The overall effect is the gradual development of cardiopulmonary diseases that, over many years, lead to death. Acute level 4 penetration can also lead to premature death for persons already suffering from cardiopulmonary diseases.

Table 2.1: Penetration levels of particulate matter into the human respiratory system and their impact on human health (Gunter, 1999).

	Averaging Period	U.S.	B.C.
PM_{10}		As of 1987	As of 1995
	24-hours	150 $\mu g\ m^{-3}$	50 $\mu g\ m^{-3}$
	1 year	50 $\mu g\ m^{-3}$	-
$PM_{2.5}$		As of 1997	*Recommended
	24-hours	65 $\mu g\ m^{-3}$	15 $\mu g\ m^{-3}$
	1-year	15 $\mu g\ m^{-3}$	-

Table 2.2: Regulatory standards of PM_{10} and $PM_{2.5}$ for the United States and British Columbia. *These regulations are not yet in effect.

2.3. PM_{10} Sources and Sinks

Most research has focused on mass and/or chemical partitioning of PM_{10}. The purpose of such studies is to identify potential sources for concentrations monitored in an area of interest. This is usually accomplished by the use of receptor models that utilise ambient air samples either from various sites (multivariate method) or from one site but coupled with various at source samples (chemical mass balance method) (Hosiokangas et al., 1999). Results differ but identified sources tend to include soil dust, road dust, combustion processes (mobile and stationary), biomass burning (natural, agricultural, and domestic), food cooking, salt spray, and gas-to-particle conversion (Hosiokangas et al., 1999; Magliano et al, 1999; McKendry, 2000; McKendry and Lundgren, 2000). Although sources can be identified, significant differences often exist between ambient measurements and emissions (Magliano et al., 1999).

The degree to which each source contributes to total concentrations varies with location and time. Small scale spatial and temporal variations are not well understood, however, more general relationships have been observed. Rural concentrations are usually dominated by soil dust and biomass burning (Clark *et al.*, 1999) while urban centres have higher proportions originating from road dust and combustion processes (Clark *et al.*, 1999; McKendry, 2000).

Differences between rural and urban sources are more distinct in regions with low population densities where urban centres are isolated (Hoek *et al.*, 1997). In densely populated regions, such as Europe, rural areas are usually at close proximity with several urban centres and, consequently, differ less in their pollution profiles (Hoek *et al.*, 1997). Temporal variations are largely dependent on meteorology.

Anthropogenic sources generally emit a higher proportion of fine-mode particles ($PM_{2.5}$) than natural sources. Urban PM_{10} is largely (70-90%) composed of $PM_{2.5}$ because urban emissions are dominated by anthropogenic sources (Keywood *et al.*, 1999) Magliano *et al.*, 1999; Zheng *et al.*, 2000). Therefore, urban sources, in addition to emitting greater total quantities, are in themselves more hazardous (McKendry, 2000).

The variety of sources responsible for PM_{10} cause the pollutant's mass distribution to be multi-modal. Figure 2.2 illustrates an idealised mass distribution of atmospheric particulate matter. The mass distribution, however, is usually site-specific and may also depend on meteorology (correlation between PM_{10} and meteorological parameters is discussed in the next section). Table 2.4 lists examples of observed mass distributions for various site types.

True PM_{10} sinks, that is, processes that extract PM_{10} from the atmosphere, are poorly understood. They are assumed to be both wet and dry deposition (Querol *et al.*, 1998) as well as particle volatilisation (McKendry, 2000). Wet deposition may behave as a sink by depleting clouds of condensation nuclei and by adsorbing particles on the surface of raindrops, snow flakes, or hail stones (Querol *et al.*, 1998). Dry deposition simply refers to the mechanical deposition that occurs when the horizontal velocity of the load is reduced below the settling velocity of the particle. Deposition is deemed a permanent sink as re-suspension of particles is incorporated as a source (Hosiokangas *et al.*, 1999). Volatilisation is the change in the phase of

a particle from solid or liquid to gas (particle-to-gas conversion). Volatilisation may be considered a permanent sink because its inverse process, gas-to-particle conversion, is also included as a source.

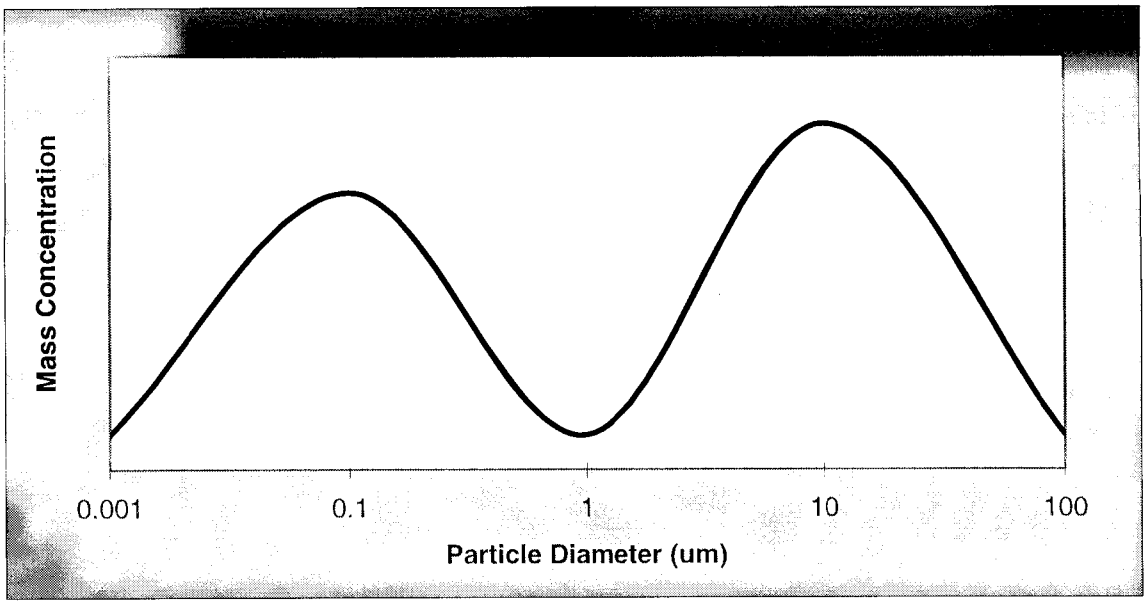

Figure 2.2: Idealised mass distribution for atmospheric particulate matter (after Arya, 1999)

It is logical to assume that particles are eventually deposited or volatised. The rate at which these processes occur, however, is unknown. Dry deposition rates have been estimated by Blanchard *et al.* (1999) and Kleeman *et al.* (1999) and have given successful results but the rates were not presented. Volatilisation rates do not appear in the literature.

Location	Condition	Particle Size Range (μm)	Location of modes (μm)	Researchers
Wallops Island, VA	Marine Modified marine	0.006 – 2.2	0.2; 8 0.03; 0.1; 6	Hoppel et al. (1990)
Tasmania	Marine Modified marine	0.005-5	0.025; 1	Gras and Ayers (1983)
Brisbane	Traffic influenced	0.016-30	0.2; 3	Morawska et al. (1998)
South Africa	Background Fires	0.1-3	0.2-0.4; 1; 3 0.2-0.3; 3	LeCanut et al. (1996)
Budapest	Suburban	0.02-100	0.2; 20	Meszaros (1977)
Southern California	Background Traffic influenced Desert Marine	0.015-30	0.5; 4 0.025; 0.25; 2.5 0.4; 8 0.5; 10	Hidy (1975)
Tasmania and Hawaii	Marine Modified marine	0.17-7.5	2 0.2; 2	Porter and Clark (1997)

Table 2.3: Examples of particle diameter mode location(s) in particle mass distributions for various site types for various site types (after Morawska et al., 1999)

2.4. Air Pollution Meteorology in Coastal Regions with Complex Terrain

Ozone, the major component of photochemical smog, is perhaps the most researched lower atmospheric pollutant. For this reason, ozone research is used here to provide an overview of pollution meteorology. The combination of mechanisms that affect ozone distribution varies

with time and location as it is dependant on synoptic meteorology, terrain type, and proximity to large water bodies. It is beyond the scope of this paper to describe every potential scenario, therefore, the focus is placed on coastal cities with complex terrain during summer anticyclonic conditions. This scenario is selected because (a) summer anticyclonic conditions are often associated with high ozone concentrations (McKendry, 2000), (b) coastal cities with complex terrain have perhaps the most intricate combination of processes (Pisano *et al.*, 1997), (c) a significant proportion of the population reside in coastal cities and many of these have complex terrain (Steyn, 1996) and, (d) the location of the work presented in later sections is a coastal region with complex terrain. Figure 2.3 may be used as a reference for the remainder of this section.

Anticyclones are high pressure systems with pressures decreasing outwards to its periphery. The pressure gradient is usually weak hence subsiding air moves slowly outwards resulting in stagnant conditions (Flohn, 1969). Subsidence limits the height of the mixed layer (ML) (Stull, 1988; McKendry, 2000) which is developed during the day when the near surface air is heated (Stull, 1988). The reduced depth of the ML and the stagnant conditions cause poor vertical and lateral dispersion of pollutants (Blanchard *et al.*, 1999). Anticyclones are also characterised by clear and warm conditions that increase ozone production - a photochemical pollutant (McKendry and Lundgren, 2000). Poor dispersion (Lu and Turco, 1995) and an increase in source strength may be partly responsible for the high ozone concentrations associated with summer anticyclonic conditions. The stagnant and sunny conditions, however, may aggravate pollution concentration in additional ways.

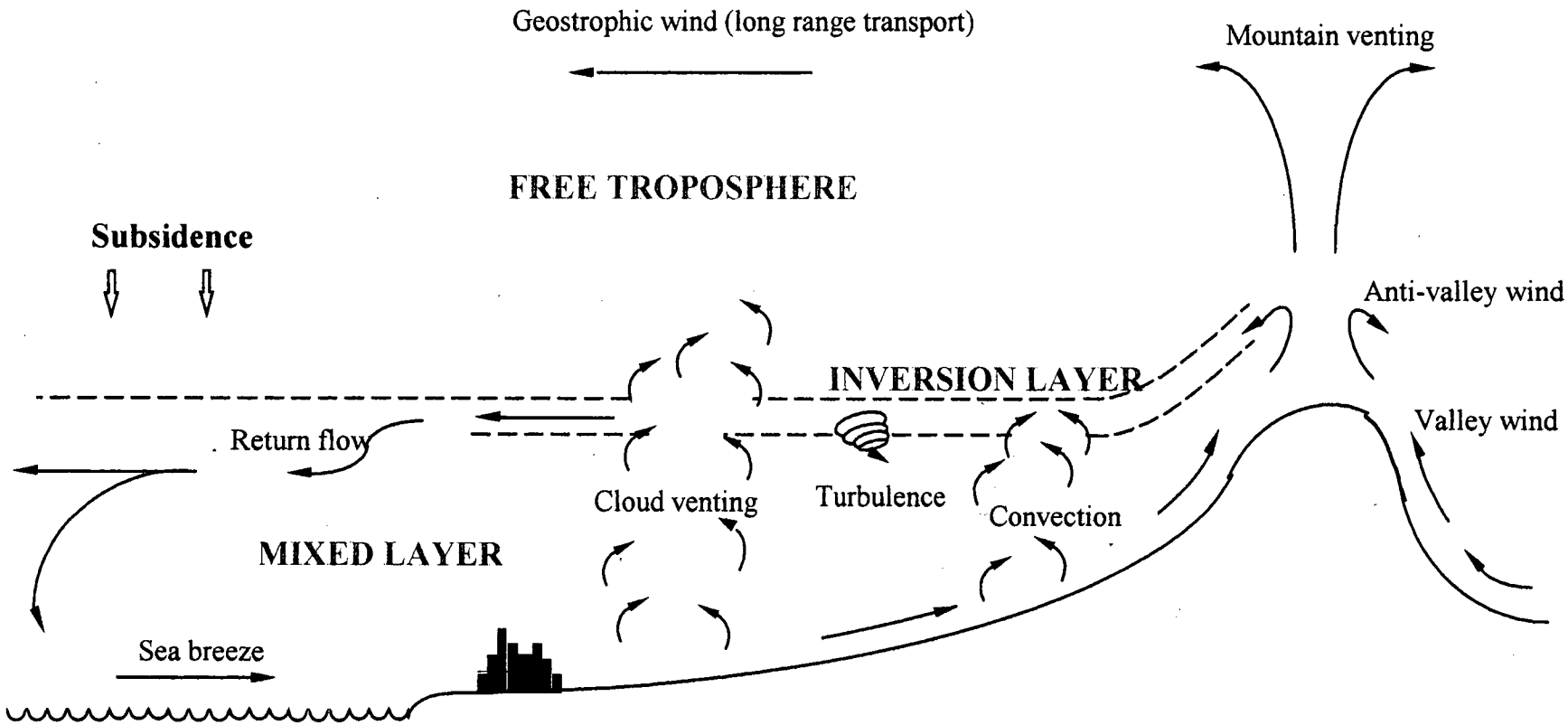

Figure 2.3: Mechanisms of pollution dispersion. Modified from McKendry and Lundgren (2000)

Strong insolation and light winds can allow the formation of a well developed sea-breeze and of mountain winds (Lalas *et al.*, 1987). The coastal plain is heated more rapidly than a nearby water body and, as a result, a pressure gradient develops between the water (high) and the coastal plain (low) causing an onshore flow (Stull, 1988). Similarly, mountain summits receive more insolation than valleys causing a pressure gradient and subsequent upslope flow (Stull, 1988; Lu and Turco, 1995). In certain cases the sea-breeze and valley winds may combine to become one continuous flow (Ulrickson and Mass, 1990; McKendry and Lundgren, 2000) that begins offshore, moves inland, and eventually reaches mountain summits (Ulrickson and Mass, 1990). This flow can transport ozone away from the city and up the mountains (McKendry and Lundgren, 2000).

Sea-breezes and valley winds are usually accompanied by overhead flows in the opposite direction. These anti-flows exist to sustain continuity (Stull, 1988; McKendry, 2000). The anti-sea-breeze and anti-valley wind may also become indistinguishable (Ulrickson and Mass, 1990). At the summit, transported ozone may be partially captured by strong thermals and be convected to the free troposphere (FT) (Ulrickson and Mass, 1990; Lu and Turco, 1995; McKendry *et al.*, 1997). This process is known as the mountain venting (McKendry and Lundgren, 2000). The remaining ozone may be seized by anti-valley winds and introduced into a stable layer between the ML and the FT referred to as the inversion layer (IL) (Ulrickson and Mass, 1990; Lu and Turco., 1995; McKendry and Lundgren, 2000). Here, ozone may be advected offshore where some of the pollutants may be re-circulated into the sea-breeze (Lu and Turco, 1995). This ongoing flow system can cause a persistent ozone layer aloft. Such layers may have ozone concentrations several times greater than those near the surface (McKendry *et al.*, 1997).

The thermal drives that create the sea-breeze and valley winds dissipate in the evening with surface cooling (Stull, 1988). As a result, the diurnal flow system stops (McKendry, 2000). During this time, a shallow and stable nocturnal boundary layer (NBL) is developed (Stull, 1988, McKendry and Lundgren, 2000). These stagnant conditions, along with the lack of solar radiation, permit the rapid depletion of ozone from surface and chemical sinks (Neu, 1995). This may give the impression that the pollution has been removed from the region. The rapid cooling of summits, relative to valleys, and of the coastal plain, relative to the water, eventually causes a pressure gradient that induces the development of a land-breeze and of mountain winds (Stull, 1988). The offshore flow carries fresh emissions away from the city and over the water (Lalas et al., 1987). The elevated pollution layer remains intact but subsidence and a shallow NBL allow it to descend (McKendry and Lundgren, 2000). Sporadic turbulence can disrupt this lower layer and cause down-mixing of pollutants aloft thus re-circulating ozone to the surface (Neu et al., 1994)

As the next day begins, nocturnal flows cease and the pollutants advected offshore undergo photochemical reactions to create ozone (Lalas *et al.*, 1987). The ML develops and intercepts the now lower ozone layer above (McKendry and Lundgren, 2000). This allows pollutants from the previous day to be re-entrained into the ML (McElroy and Smith, 1993; Neu, 1995). Furthermore; newly created offshore ozone is advected onshore with the evolution of the sea breeze (Lalas *et al.*, 1987; McKendry and Lundgren, 2000). Recycling of ozone may cause a continuous accumulation and lead to extreme pollution episodes (Lu and Turco, 1994).

Elevated ozone layers can also be fuelled by penetrative convection (McElroy and Smith, 1993; McKendry et al., 1997; McKendry and Lundgren, 2000). Penetrative convection occurs when air, heated by the ground, rises and penetrates the lower boundary of the IL (Stull,

1988; McKendry and Lundgren, 2000). If a temperature inversion is present, the convected air becomes relatively cool and sinks (Stull, 1988) leaving the convected ozone trapped in the IL (McKendry et al., 1997; McKendry and Lundgren, 2000). This can further enhance the cycling of ozone. By contrast, updrafts caused by stronger thermals or low-level wind convergence may penetrate beyond the IL (cloud venting) into the FT and act as sinks for surface ozone (Lu and Turco, 1995; McKendry and Lundgren, 2000). Convective activity may also be caused by the urban heat island effect (Lehning et al., 1998)

The possibility that pollution may be re-circulated into an area of interest may have serious implications for model development. Excluding the above mentioned dispersion processes may result in the miscalculation of source strength and, subsequently, of required emission reductions. For example; it is possible that the large offshore contribution observed by Kleeman *et al.* (1999) partly originated from within the Los Angeles Basin and not from overseas, as speculated in their results. If this is so then local source strength was underestimated in that study.

Spatial and temporal ozone distribution is not necessarily representative of PM_{10}. In fact, McKendry (2000) observed a poor correlation between the two pollutants. This may be caused by the photochemical origins of ozone. Chemical sinks that rapidly deplete ozone during the evening, in spite of poor dispersion, do not exist for PM_{10}. Increased solar radiation caused by clear conditions and solar declination increase ozone source strength during summer anticyclonic conditions. PM_{10} source strength may increase during such conditions as a result of gas-to-particle conversion that occurs during ozone production. However, this increase might be minimal and thus may explain why McKendry (2000) observed a much more pronounced increase in ozone concentration during anticyclonic events. Also, a lag-time is present with

ozone production but absent with PM_{10}. The average time for ozone formation, after emission of its precursors, is 2.5 hours causing maximum ozone concentrations to exist away from the source. By contrast, PM_{10} is a primary pollutant hence its highest concentrations are likely to be close to the source. Poor correlation may therefore stem from the nature of the pollutants rather than differences in dispersion mechanisms.

Observations of ozone vertical distribution should not be used in PM_{10} modelling as the two pollutants may in fact behave differently. Ozone research, however, can be used as a guide for future PM_{10} research. It provides a description of varying flow systems that may help in analysing future PM_{10} vertical profiles. It may also help in research design. Overall, it emphasises the need to acquire a complete and three-dimensional data set for PM_{10}.

2.5. Temporal and Spatial Behaviour of PM_{10}

Few studies have focused on correlating PM_{10} concentrations and meteorological parameters (McKendry, 2000). Findings from existing studies, however, are similar and describe relationships with precipitation, wind speed, and wind direction. Querol et al. (1998) also observed a positive correlation for relative humidity and insolation with gas-to-particle conversion, however, no explanation was offered. It is possible that water and light may contribute to the change of phase process.

Precipitation is negatively correlated with PM_{10} concentrations (Blanchard et al., 1999; Magliano et al., 1999). This is partially due to the role of precipitation as a PM_{10} sink. The negative correlation may also result from a depleted source strength as wet or snow covered surfaces are less likely to emit dust (Richards et al., 1999). The total emission reduction is

liable to be significant because, as previously mentioned, road and soil dust contribute to a large proportion of PM_{10} concentration. Low level concentrations associated with precipitation may partially explain why lowest mean seasonal concentrations tend to occur during the winter when snow or rain (depending on the region) are more frequent (Blanchard *et al.*, 1999). There are, however, exceptions (see Figure 2.4) to this seasonal variation (McKendry, 2000).

Wind speed is also negatively correlated with PM_{10} concentrations, however, this relationship may not extend to rural sites (Blanchard *et al.*, 1999; McKendry, 2000). At urban sites, stagnant conditions commonly result in elevated concentrations because the pollution is not dispersed and thus allowed to accumulate (Lu and Turco, 1995). As wind speed increases so does the carrying capacity of the air and particles that are not deposited are more apt to be transported out of the 'local' atmosphere. Querol *et al.* (1998) observed only a weak correlation with wind speed. This weak correlation, however, may have resulted from the inclusion of rural data. At rural sites, strong winds can cause significant soil dust emissions resulting in very high concentration levels (Blanchard *et al.*, 1999; McKendry, 2000). These findings do not necessarily imply a positive correlation with wind speed in rural areas. It is possible that the relationship is simply non-linear.

Wind direction is largely responsible for the spatial variation of PM_{10} concentrations (Hoek *et al.*, 1997). The influence of wind direction on concentration depends on the relative position of an area of interest to the wind direction and to pollution sources (Hoek *et al.*, 1997). Consequently, a general relationship between a specific wind direction and PM_{10} concentration does not exist.

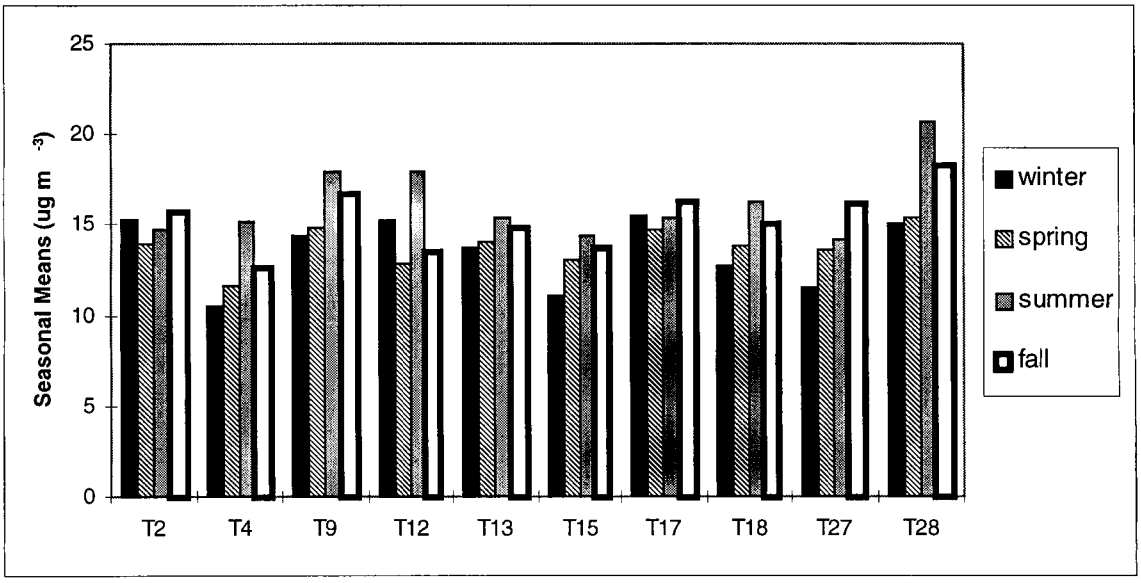

Figure 2.4: Mean seasonal concentrations of PM_{10} at ten stations in the Lower Fraser Valley. The average distance between stations is 13.4 km. Note that winter is not the season with the lowest concentration at stations T2, T12, and T17 and that it is the season with the the highest concentration at T2. Data source: McKendry (2000).

Regions are commonly dominated by a particular wind direction. In addition; complex topography can create localised wind patterns that are persistent. A persistent wind direction could cause downwind sites to experience concentration levels that are tenaciously higher relative to those of upwind sites.

Although relatively little information exists for the development of a PM_{10} model, Kleeman *et al.* (1999) have successfully applied a PM_{10} dispersion model to the Los Angeles Basin. The model is based on surface measurements of PM_{10}, basic meteorological parameters (at the surface and aloft), estimates of vertical mixing, and estimates of deposition rates. The model predicted concentration, particle size, and chemical composition well at hourly intervals. The model appears promising, however, its validity may be questioned for three reasons: (1) the model was only tested for one day, (2) predictions were only tested at three points, and (3) background concentrations were assumed to have originated overseas.

Testing the model for only one day says little about the model's ability to predict as success may be attributed to simple coincidence. The limited number of test sites offers a poor description and explanation of possible spatial variability such as that observed by Blanchard et al. (1999), Magliano et al. (1999), and McKendry (2000) (each observed a decreasing inter-station correlation with distance greater than ~20 km). This is especially true because the sites were approximately 40 km apart. The assumption that background concentrations originated overseas may be false. It is true that particulates can be carried long distances, however, there is a possibility that a significant portion of the background concentration actually originated within the basin. Altogether, this study does little to contradict the previously mentioned limitations of PM_{10} modelling.

2.6. Expected Actual Behaviour of PM_{10} in the Vertical

It has been mentioned several times that PM_{10} may not behave homogeneously in the vertical. That is, the larger particles may be settling out, even during well mixed conditions, while smaller particles may become well mixed throughout the boundary layer. There are no observations to confirm this hypothesis, however, an analogy to profiles of suspended sediment in rivers may be used to examine the potential structure of PM_{10} in the vertical.

PM_{10} particles are so small that their free fall in the atmosphere is more closely related to that of sediments in water than to that of larger objects free falling in the air (Serway, 1996). If the atmosphere of interest is located in the boundary layer of a valley, then the best comparison is to suspended sediment in a river. The terminal velocity of a sediment particle determines how far that particle can travel (Pye, 1994). The terminal velocity, in turn, is determined primarily

by the particle's mass and shape. If a constant density and shape are assumed, then larger particles have a higher terminal velocity, that is, they can accelerate downward longer than smaller particles. In addition, greater upward force is required to lift the particle. The result is a sediment concentration gradient that decreases with decreasing particle size (see Figure 2.5). Although the transportation medium differs for PM_{10}, size-segregated profiles within the boundary layer could be expected to show similar characteristics.

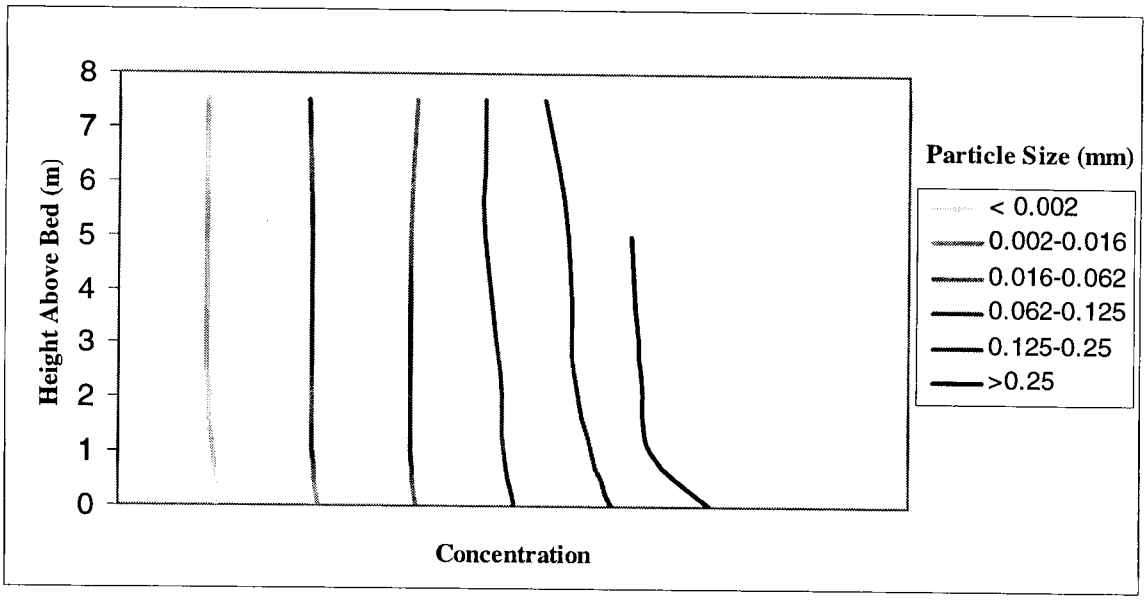

Figure 2.5: Size-segregated vertical profiles of suspended sediment in the Mississippi River After Colby (1963)

2.7. Conclusion

The ultimate purpose of air quality research is to develop dispersion models that accurately describe the processes influencing pollution concentration within a given area (Magliano et al., 1999). By describing these processes, dispersion models allow legitimate

assessments for emission abatement policies (Magliano et al., 1999). The development of such models requires extensive monitoring of pollution concentrations and meteorological parameters in three dimensions (Kleeman et al., 1999). Also; a quantitative understanding with respect to sources and sinks is required (Kleeman et al., 1999). The state of knowledge for PM_{10} is clearly not sufficient for the development of accurate dispersion models.

The emission inventories acquired provide the most complete portion of the PM_{10} knowledge. These data, however, are used to provide source strength and do not in themselves explain dispersion processes. The existing basic relationships with meteorological parameters are liable to only explain broad spatial and temporal variations. Wind speed and direction may fail to explain local variations that may be dominated by turbulence, convection, or eddies (Neu et al., 1994). A very meagre understanding of sinks may also impair model development as dispersal distances are partially dependent on particle lifetime.

A good understanding of PM_{10} dispersion may also be restricted by the lack of above surface data. Current research on other pollutants suggests that obtaining vertical measurements of PM_{10} may be necessary to achieve a clear understanding of surface concentrations (Pisano et al., 1997). Vertical observations of ozone have detected the existence of elevated ozone layers that may allow the pollutant to be re-circulated to the surface (McElroy and Smith, 1993; Neu et al., 1994; McKendry et al., 1997; McKendry and Lundgren, 2000). Ozone is a photochemical gas and may behave differently than PM_{10} but the processes that govern its vertical distribution may be similar to those that influence PM_{10}. Consequently, it is important to inspect these processes because they may serve as a guide for future PM_{10} research. In all; PM_{10} modelling may be limited, at this time, to producing very coarse statements at the regional and seasonal scale.

Chapter III: Instrumentation and Methodology

3.1. Introduction

There is little known about the vertical distribution of PM_{10} with respect to concentration and, even more so, with respect to particle size. This gap in PM_{10} research may largely result from a lack of suitable instruments. In order to measure PM_{10} in the vertical, an instrument must possess four basic qualities: (1) it must be automated; (2) it must record measurements at a sufficiently fine temporal resolution to deal with the dynamic nature of the atmosphere; (3) it must be portable, in terms of its physical structure and its sensitivity to a changing environment, so that it may be launched by balloon or attached to an aircraft; (4) it must be able to identify particle size (diameter), and measure more than one size, so that only particles less than 10 μm are included in the measurement. If a vertical size distribution is desired, then the instrument must also be able to classify PM_{10} into various size categories.

All existing measurement systems for ambient particulate matter lack one or more of the above-mentioned qualities. Routine monitoring instruments, usually consisting of a variety of filters, can separate particles according to size but they are not computerized and their structure renders them stationary (Chow, 1994; Ayers et al., 1999). The tapered element oscillating microbalance (TEOM) is a gravimetric instrument that is automated and can record measurements at a fine temporal resolution (2 seconds) but it is not portable (Ayers et al., 1999). Remote sensing instruments are portable, automated, and can record measurements several times per second. They have, in fact, been used to obtain vertical measurements of particulate matter (Wakimoto and McElroy, 1986; Hoff et al., 1996; Ferrare et al., 1998; Hamonou et al.,

1999). These instruments, however, either detect the presence of all particulate matter or record the concentration of particles with a specific diameter. Lidar is the most commonly used remote sensing instrument for particulate matter. It measures concentrations of particles with a diameter of 1 μm only and thus is only representative of PM_{10} if the particle size distribution is homogeneous. Aerosol spectrometers falter with their lack of mobility. Spectrometers are generally too large and heavy to be suitable for airborne measurements. One potential exception is the GRIMM Particle Dust Monitor.

3.2. The GRIMM Particle Dust Monitor 1.108

The GRIMM Particle Dust Monitor (model 1.108) is a portable aerosol mass spectrometer having dimensions of 24 x 12 x 6 cm and a mass of 1.7 kg (see Plate 1). It is capable of measuring particulate matter in terms of particle count (particles per litre) or mass concentration ($\mu g\ m^{-3}$). Measured particles can range from 0.3 to greater than 20 μm in diameter and can be sorted into fifteen size classes specified by the user. The GRIMM can measure every six seconds (if connected to a computer) or every minute and can store approximately 40 hours of data on a memory card. The data are exported to a computer via a data interface (model RS-232C). (GRIMM Labortechnik Ltd., 1996)

The GRIMM samples air using an isokinetic pump. The air enters the instrument at a constant flow rate ($1.2\ l\ min^{-1}$) and initially passes through a sample cell containing a laser diode light beam and a photo diode detector. The passage of particles in the sample cell scatters the light beam at angles dependant on particle size. The detector quantifies the angular dispersion to obtain a particle size distribution and, subsequently, amplifies the signal to a pulse

height analyser. The analyser classifies the particles according to size and estimates the mass concentration, for each class, according to particle size, particle count, and the fixed volume provided by the isokinetic pump. The sampled air exits the sample cell and passes a Teflon filter before exiting the GRIMM. The filter collects all sampled particles greater than 0.3 μm in diameter that can be weighed (manually at the end of a run) to obtain the actual total mass sampled throughout the run. The filter value may be entered in the instrument software (GRIMM 1.174) to provide a correction factor for self-calibration. More detailed information on the GRIMM may be found in Appendix I. (GRIMM Labortechnik Ltd., 1996)

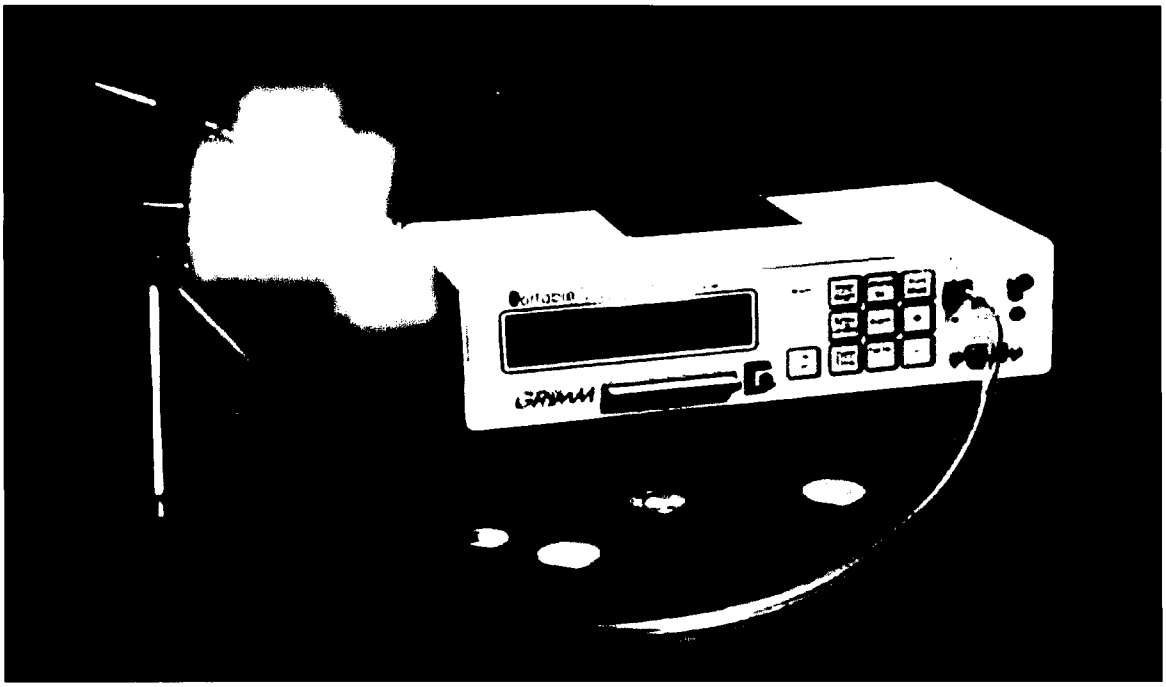

Plate 1: The GRIMM Particle Dust Monitor 1.108

Calibrating the GRIMM for site-specific measurements is necessary for two main reasons. First, particles with diameters smaller than 0.3 μm are neglected hence the instrument consistently underestimates mass concentration. The magnitude of this error depends on the

average particle size distribution for a given site. Second, the GRIMM uses a constant particle density to estimate mass and thus mass concentration. This simplification may result in either positive or negative error depending on the local particle composition. Although site-specific calibration is possible using the GRIMM's Teflon filter, the application of this method is not practical. The pump samples a relatively small volume of air and ambient mass concentrations are usually low. The total mass that accumulates on the filter is thus minimal. Obtaining an accurate correction factor therefore requires microanalysis of the filter. It is, by comparison, more practical to calibrate the GRIMM with a calibrated instrument.

The GRIMM dust monitor is, overall, the most promising instrument for obtaining vertical measurements of PM_{10}. However; the manner by which it estimates mass concentration may be an obstacle to vertical profiling. As previously mentioned, the mass concentration is estimated, in part, by a fixed volume of air provided by the isokinetic pump. The pump, however, requires manual adjustments to cope with varying wind speeds. Wind speeds greater than the pump's capacity may cause an acceleration of the sampling flow rate used to estimate mass concentration and, consequently, increase instrument error.

Manual adjustments are impossible after the instrument is launched. Wind speed generally increases with elevation so, as the GRIMM ascends, it may encounter wind speeds greater than the pump's capacity. As a result, the vertical size distribution observed may not be representative. The degree to which wind speed affects the instrument flow rate was therefore an important consideration prior to field deployment.

Relative humidity changes may also increase instrument error. Water can accumulate on the surface of particles and the accumulation increases with increasing relative humidity (Raunemaa and Bernotas, 1994; Meng et al., 1995;). The photo diode detector includes water as

part of a particle's size and estimates its mass accordingly (Reponen et al., 1996; Gebhart, 1992;). Relative humidity causes this form of error with most optical and remote sensing instruments. In conditions of high relative humidity (greater than 95%) the error may be as high as 30% (Gebhart, 1992). Past attempts at using the GRIMM as a monitoring device have established it to be unreliable during rainy conditions i.e. the instrument largely overestimates the mass concentration. However, the manufacturer does warn that the GRIMM can only adequately dry the sampled particles when relative humidity is below 95%. Use of the GRIMM should therefore be limited atmospheric conditions having a relative humidity lower than 95%. The use of tethered balloons is usually restricted during rainy or overcast conditions i.e. high relative humidity conditions. Instrument problems related to relative humidity should not be neglected but are not likely to be a major concern with deployment on a tethered balloon.

3.3. Deployment on a 5 m^3 Tethered Balloon

The maximum lift of a 5 m^3 tethered balloon at 1 km above the surface is approximately 3 kg. In order to gain height information and to interpret the profiles obtained, vertical measurements of meteorological variables and PM_{10} concentrations must be taken simultaneously. Consequently, the balloon must lift both the GRIMM and a meteorological package. The overall weight (see Table 3.1) caused some concern about lift potential. To adjust the weight, the GRIMM's rechargeable battery was replaced by a battery pack containing disposable batteries. The combined weight was reduced enough to allow lift up to 1 km above the surface.

Instrument	Weight (kg)	
GRIMM	1.7	1.7
GRIMM battery	0.7	———
Met package	0.25	0.25
Battery Pack	———	0.4
Total weight	2.65	2.35

Table 3.1: Weight inventory for tethered helium balloon

Balloon ascent/descent sequences up to 1 km are typically very rapid (approximately 30 minutes) so that each profile is taken within the vertical circulation time of thermals. The speed of the ascent/descent sequence when using the GRIMM needs to be compromised because of the instruments relatively poor temporal resolution. To allow sufficient resolution of observations, the ascent/descent sequence must be slowed to approximately 70 minutes. Since GRIMM measurements are taken at 1-minute intervals, a 70 minute sequence up to 1 km provides two profiles with vertical spatial resolutions of 28.5 m. This is less than half of the spatial resolution typically achieved with tethered balloon profiles, however, it is considered adequate.

3.4. Laboratory tests with the GRIMM Particle Dust Monitor

Primary concern in deployment of the instrument was the variability in wind speeds encountered during profiling. The GRIMM is equipped with four intakes, each suitable for a different wind speed (0.5, 1.0, 2.0, and 4.0 m s^{-1}). The range of suitable wind speed for each intake is not specified by the manufacturer. Wind speeds encountered while using a 5 m^3

tethered balloon up to 1 km above the earth's surface do not usually exceed 6 m s^{-1} for two reasons: (1) the clear conditions required for deployment of a tethered balloon are usually accompanied by calm (essentially no wind) or near-calm conditions and (2) sufficient control and lift of a 5 m^3 tethered balloon become problematic with wind speeds greater than 6 m s^{-1}. Because only a single inlet can be used during airborne measurements, it is necessary to test each inlet for its ability to sample within a range of 0 to 6 m s^{-1}.

Ideally, the testing of each inlet would occur in a completely controlled environment, that is, where the wind speed and particle concentration were controlled at all times. Unfortunately, facilities allowing such a controlled environment were not available for this work. Testing was consequently performed with a wind tunnel at the University of British Columbia. The wind tunnel is located in a closed room that was assumed to contain a relatively constant particle concentration during a short time period (two days).

The data were collected on 5 and 6 January, 2001. At the beginning of each day, the wind tunnel was turned on to maximum capacity (7 m s^{-1}) for two hours to assure the entrainment of all particles from the tunnel's inner walls. This was to avoid entrainment occurring during testing and thus changing the particle concentration within the room. The GRIMM was subsequently placed within the wind tunnel to measure for a period of 20 minutes, at 6 second intervals, for each inlet. The series of measurements was carried out with the tunnel set to 0, 0.5, 1, 2, 4, and 6 m s^{-1}. The choice of wind speeds is meant to represent both the range expected during airborne measurements and the specified suitable speed for each intake.

Assuming the particle population in the room remains constant, an intake suitable for a given wind speed range should provide consistent results when measurements are taken within that range. Similarly, if all intakes are suitable for the same range then measurements obtained

with one intake should not be significantly different from those obtained with another intake.

To test for potential deviations between intakes, or between wind speeds for a single intake, a series of two-sample difference-of-proportion tests were performed (see Table 3.2 and Table 3.3). Each test was set for a two-tailed hypothesis, that is, to test for any difference between the two samples. The test assumes that the populations sampled are consistent and normally distributed.

Intakes Compared	Wind Speeds ($m\ s^{-1}$) Tested
4 $m\ s^{-1}$ and 0.5 $m\ s^{-1}$	0, 0.5, 1, 2, 4, and 6
4 $m\ s^{-1}$ and 1 $m\ s^{-1}$	0, 0.5, 1, 2, 4, and 6
4 $m\ s^{-1}$ and 2 $m\ s^{-1}$	0, 0.5, 1, 2, 4, and 6

Table 3.2: Two-sample-difference-of-proportion tests performed between intakes.

Intake Tested	Wind Speeds Compared ($m\ s^{-1}$)					
4 $m\ s^{-1}$	0	0.5	1	2	N/A	6
2 $m\ s^{-1}$	0	0.5	1	N/A	4	6
1 $m\ s^{-1}$	0	0.5	N/A	2	4	6
0.5 $m\ s^{-1}$	0	N/A	1	2	4	6

Table 3.3: Two-sample-difference-of-proportion tests performed between wind speeds for each intake.

The results of these tests, discussed in Chapter 4, essentially determine the GRIMM's potential for deployment on a tethered balloon. At least one inlet must be found suitable for the expected wind speed range. If not, then suitable conditions for deployment (already limited to clear and relatively calm situations) would be further restricted. If each inlet demonstrates a very narrow range of suitability, the GRIMM cannot be used at all for vertical profiling.

3.5. Calibration

As previously mentioned, calibration of the instrument is essential as mass concentrations are estimated from a single density. In addition; the GRIMM is limited to particles with a diameter greater than 0.3μm. Since particle mass distributions typically show a mode at 0.1 μm, it can be assumed that a considerable amount of mass is excluded from the measurements. The GRIMM's ability to take accurate real time measurements is also a concern. Due perhaps to poor translation, the instrument manual does not clarify whether each measurement is taken independently or if there is some dependence on previous measurements (in a form of running average). To observe potential error, the GRIMM was compared to two instruments, described below.

Tapered-Element Oscillating Microbalances (TEOMs) are regularly used in particulate matter monitoring networks. Air sampled by a TEOM passes through a filter, where particulate matter collects, and then continues through a hollow tapered element towards an active volumetric flow control system. The instrument monitors particulate matter using an inertial balance that directly measures the mass collected on a filter by monitoring the corresponding frequency changes of a tapered element. Because the TEOM measures true mass, it is adequate for gravimetric comparison with the GRIMM.

Simultaneous measurements of PM_{10} and $PM_{2.5}$ were taken with the GRIMM and TEOM (provided by the GVRD) at Vancouver International Airport (Figure 3.1) on five days (see Table 3.4 for dates and times). Measurements with the GRIMM were taken at 1-minute intervals to correspond with the 1-minute average data of the TEOM. The GVRD monitoring station is located approximately 500 m from a main runway presumably allowing for a

substantial source of particulate matter. The GRIMM was placed 1 m away from the TEOM intake (located on the rooftop of a shed). The distance between instruments naturally results in minor sampling differences, however, these should be negligible.

To observe the GRIMM's ability to take accurate measurements at high temporal resolution and in changing conditions, the instrument was compared to a Passive Cavity Aerosol Spectrometer Probe (PCASP). The PCASP detects single particles and sizes them by measuring the intensity of light that the particle scatters when passing through a light beam. A Helium Neon laser beam is focused to a small diameter at the centre of the instruments inflow. Particles crossing the beam scatter light in all directions and some of this light is collected by a mangin mirror. This collected light is transmitted to a photodetector and then amplified, conditioned, digitised, and classified into various size classes. The size of the particle is determined by measuring the light scattering intensity and using Mie scattering theory to relate this intensity to the particle size. The main difference between the PCASP and the GRIMM is that the PCASP analyses each particle sampled individually while the GRIMM analyses a collection of particles.

Simultaneous, size-segregated measurements were taken at Sumas Mountain on 27 and 28 August, 2001 between 08:40-16:05 PDT and 14:45-17:40 PDT respectively. The site was selected solely because of the availability of a PCASP. Data were collected, using the 4 m s^{-1} intake at 5-minute intervals to correspond with PCASP measuring frequency. Although both instruments provide output in various size-classes, only eight bins have some overlap (Table 3.5). The minor differences in bin sizes should create systematic deviation between the time series, however, the focus of this comparison is to observe the correlation between the two series.

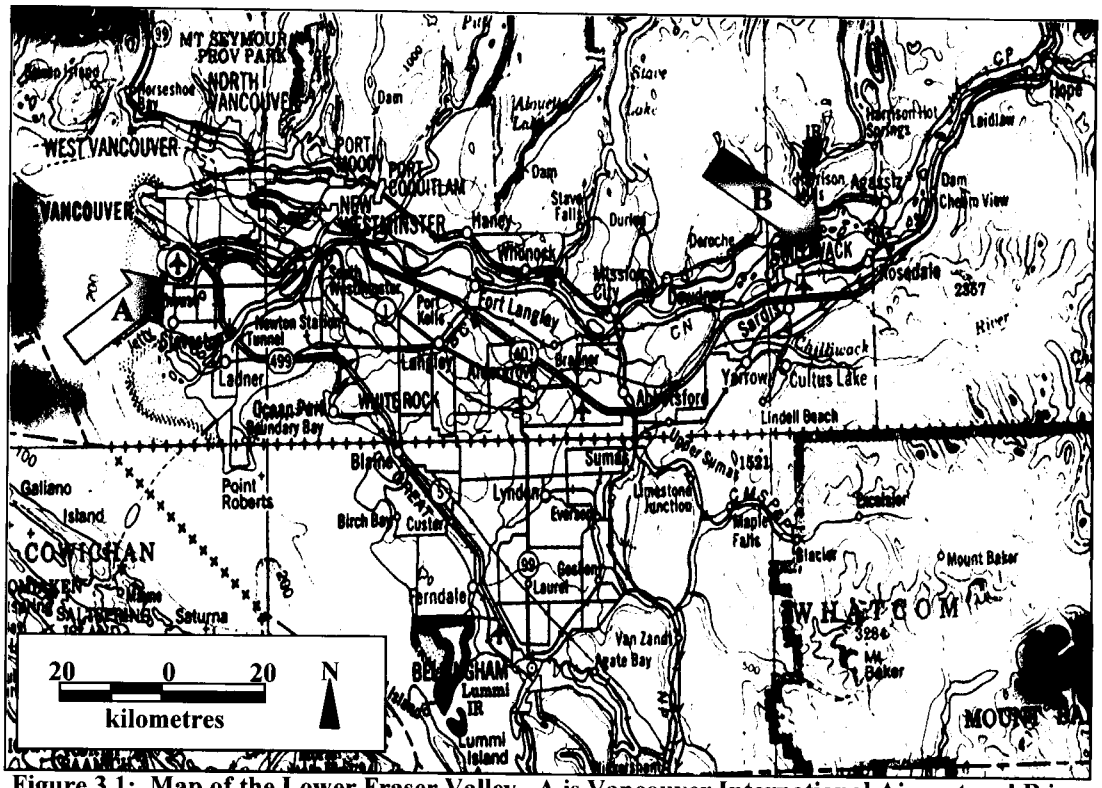

Figure 3.1: Map of the Lower Fraser Valley. A is Vancouver International Airport and B is Sumas Mountain.

June 18	June 19	June 19	June 28	July 3
11:58 – 17:00	01:00 – 05:59	11:46 – 16:46	11:01 – 16:42	11:25 – 14:22

Table 3.4: Dates and times of TEOM and GRIMM observations.

PCASP Bin (μm)	0.29 – 0.425	0.425 – 0.55	0.55 – 0.6	0.6 – 0.9	0.9 – 1.2	1.2 – 1.5	1.5 – 2.0	2.0 – 3.0
GRIMM Bin (μm)	0.3 – 0.4	0.4 – 0.5	0.5 – 0.65	0.65 – 0.8	0.8 – 1.0	1.0 – 1.6	1.6 – 2.0	2.0 – 3.0

Table 3.5: Comparison of overlapping bin sizes. The sizes are not identical but similar enough to allow the correlation of time series between instruments.

3.6. Lidar

During the field campaign (presented in Chapter 5), a scanning Lidar facility known as RASCAL (Rapid Acquisition Scanning Aerosol Lidar) was used to provide fast elevation scanning profiles of the lower troposphere with a resolution of 3 m along the laser beam axis (Strawbridge et al., 2001). RASCAL data provides a comprehensive optical picture of the atmosphere in three dimensions. This helps interpret the temporal variation of particulate matter optical properties within a widely inhomogeneous atmosphere. The basic components of a scanning Lidar system consist of a laser, beam directing/collection optics and a telescope with a detection package to convert the signal into the appropriate information that can be processed, displayed and saved in real time. Although the scanning mirror is capable of scan speeds of 24 degrees/second it was set to 0.2 degrees/second (0.4 degrees/second laser beam speed) at Langley and 0.1 degrees/second at Pitt Meadows. With a 10Hz laser this corresponds to approximately 3 and 6 min for Langley and Pitt Meadows respectively for a typical elevation scanning profile from 3 degrees above the horizon to 70 degrees. The slow scan speed was chosen to improve the solid angle resolution at distances of several kilometers from the source.

3.7. Summary

The lack of information regarding the vertical distribution of PM_{10} is largely due to a shortage of instruments suitable for airborne measurements. The GRIMM Particle Dust Monitor may be appropriate for deployment on a tethered balloon which would allow the measuring of vertical profiles. There are potential problems associated with this instrument

with respect to vertical profiling. Of greatest concern is the instrument's sensitivity to varying wind speed. To assure that accurate measurements can be taken within an expected wind speed range, the instrument was tested at several wind speeds using all speed-specific intakes provided by the manufacturer.

In addition to wind sensitivity testing, the GRIMM required calibration for three main reasons: (1) it does not measure particles with diameters smaller than 0.3 μm thus neglecting a substantial portion of the mass concentration, (2) it uses a single density to estimate mass causing its output to deviate from the true mass concentration, and (3) its ability to take independent real-time measurements is unclear. To address these problems, gravimetric comparisons were made with a TEOM and time series comparisons were made with a PCASP. The results from these comparisons, as well as from wind sensitivity tests, are presented in the next chapter.

Chapter IV: Instrument Calibration

4.1. Introduction

The previous chapter provided a description of the GRIMM Particle Dust Monitor 1.108 and addressed concerns regarding its suitability for measuring vertical profiles of particulate matter. In addition; methods of testing and calibrating the GRIMM were presented. This chapter presents and discusses the results from wind sensitivity testing and calibration.

The results presented here essentially satisfy the first objective of this work. Determining whether or not a GRIMM may be used for vertical profiling is not only important for this work but for all PM_{10} research. The instrument would provide a robust and cost-efficient method of measuring mass concentration in the vertical. In addition; validation of the instrument can also make it desirable for routine monitoring which, considering the instrument's relatively low cost, may promote an increase in network spatial resolution.

4.2. Sensitivity to Varying Wind Speed

Wind tunnel testing was performed to determine which GRIMM intake, if any, was suitable for wind speeds ranging from 0-6 m s^{-1}, that is, the wind speed range expected during vertical profiling. Since elevated wind speeds are the greatest concern, more emphasis was placed on the 4 m s^{-1} intake (it is close to the expected environmental mean during deployment). Table 4.1 shows the P-values (probability that two samples differ significantly from each other)

obtained from the two-sample-difference-of-proportions tests comparing the 4 m s^{-1} intake to all other intakes at various wind speeds. All P-values are lower than 0.05 hence indicating that measurements obtained with the 4 m s^{-1} intake and three other intakes are not significantly different from each other. This suggests that the choice of intake for a wind speed range of 0-6 m s^{-1} is irrelevant. This result, however, does not determine whether elevated wind speeds force the intake flow beyond the pump's capacity.

	Wind Speeds (m s^{-1})					
Intakes	0	0.5	1	2	4	6
4 m s^{-1} and 0 m s^{-1}	3.0 E-18	8.5E-6	6.6E-11	2.2E-42	4.7E-62	3.7E-8
4 m s^{-1} and 0.5 m s^{-1}	1.8E-15	1.0E-15	2.6E-8	7.5E-42	3.5E-60	5.5E-7
4 m s^{-1} and 2 m s^{-1}	7.2E-24	9.6E-30	4.5E-6	1.9E-31	1.2E-61	9.4E-4

Table 4.1: P-values calculated from two-sample-difference-of proportion tests.

To observe the suitability of each intake to the expected range of wind speed, two-sample-difference-of-proportions tests were used to compare measurements obtained with each intake during its 'ideal' speed and all other tested speeds. If the intake is not suitable for such a large range, then measurements obtained with the intake's ideal speed should become significantly different from measurements obtained outside of the intake's true range. Table 4.2 presents the P-values calculated from these tests. From all the tests, only two results show a significant difference. There is no real logic in where the differences occur (compared to the lack of significant difference with the other tests). In addition; the P-values are not very large. Consequently, those two results are neglected and it is concluded that all intakes are suitable for the expected wind speed range.

In spite of the test results, visual comparison of the mean concentrations observed with each inlet at different wind speeds does show small differences (Figure 4.1). The 4 m s^{-1} intake shows a clear deviation from the rest. However, this intake was the only one tested on the second day when, it was later discovered, building renovations took place in a nearby room. Concentrations appear higher at the maximum wind speed for all inlets. Although it is a concern that higher wind speeds will cause the instrument to overestimate by forcing air into the pump faster than its sampling rate, this does not appear to be the cause. The particle size distribution at different wind speeds (Figure 4.2) shows an increase in large particles with increasing wind speed yet no substantial difference in the smaller particle signatures. This suggests that the maximum wind speed tested was simply capable of entraining larger particles from surfaces within the room. The trend is therefore more likely caused by an uncontrolled environment.

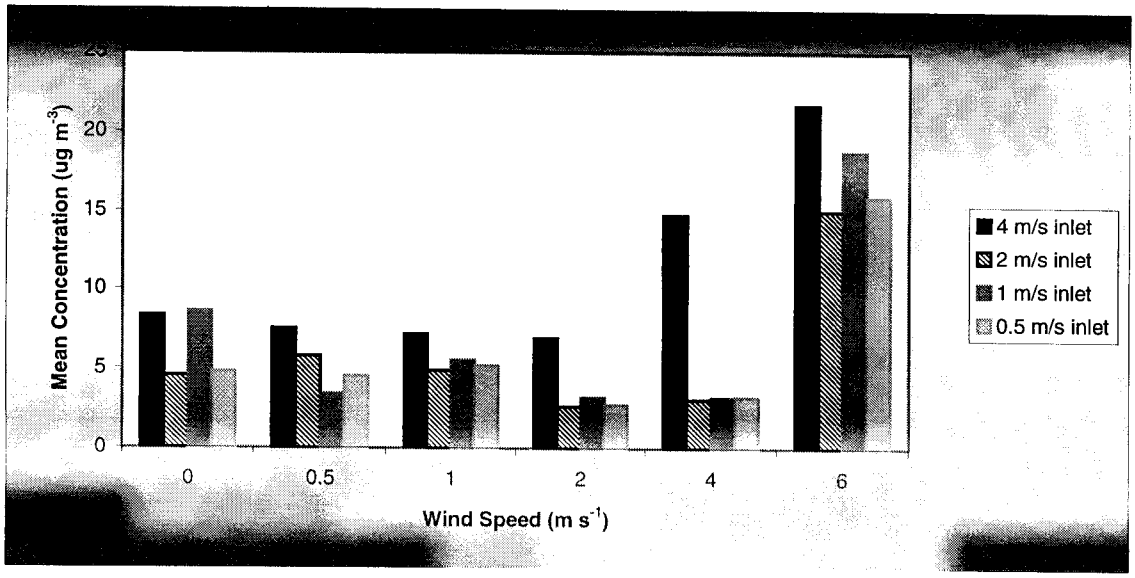

Figure 4.1: Comparison of mean concentrations of PM_{10} observed with different intakes at different wind speeds.

Intake Tested	Wind Speeds Compared ($m\ s^{-1}$)					
	0	0.5	1	2	4	6
4 $m\ s^{-1}$	1.3E-14	1.5E-18	4.7E-21	1.4E-22	N/A	1.1E-9
2 $m\ s^{-1}$	1.3E-13	5.6E-24	1.0E-17	N/A	0.16	8.6E-56
1 $m\ s^{-1}$	5.4E-7	7.8E-23	N/A	1.0E-13	6.1E-15	6.9E-37
0.5 $m\ s^{-1}$	0.10	N/A	1.5E-2	9.7E-10	8.3E-6	8.7E-28

Table 4.2: P-values calculated from two-sample difference of proportion tests.

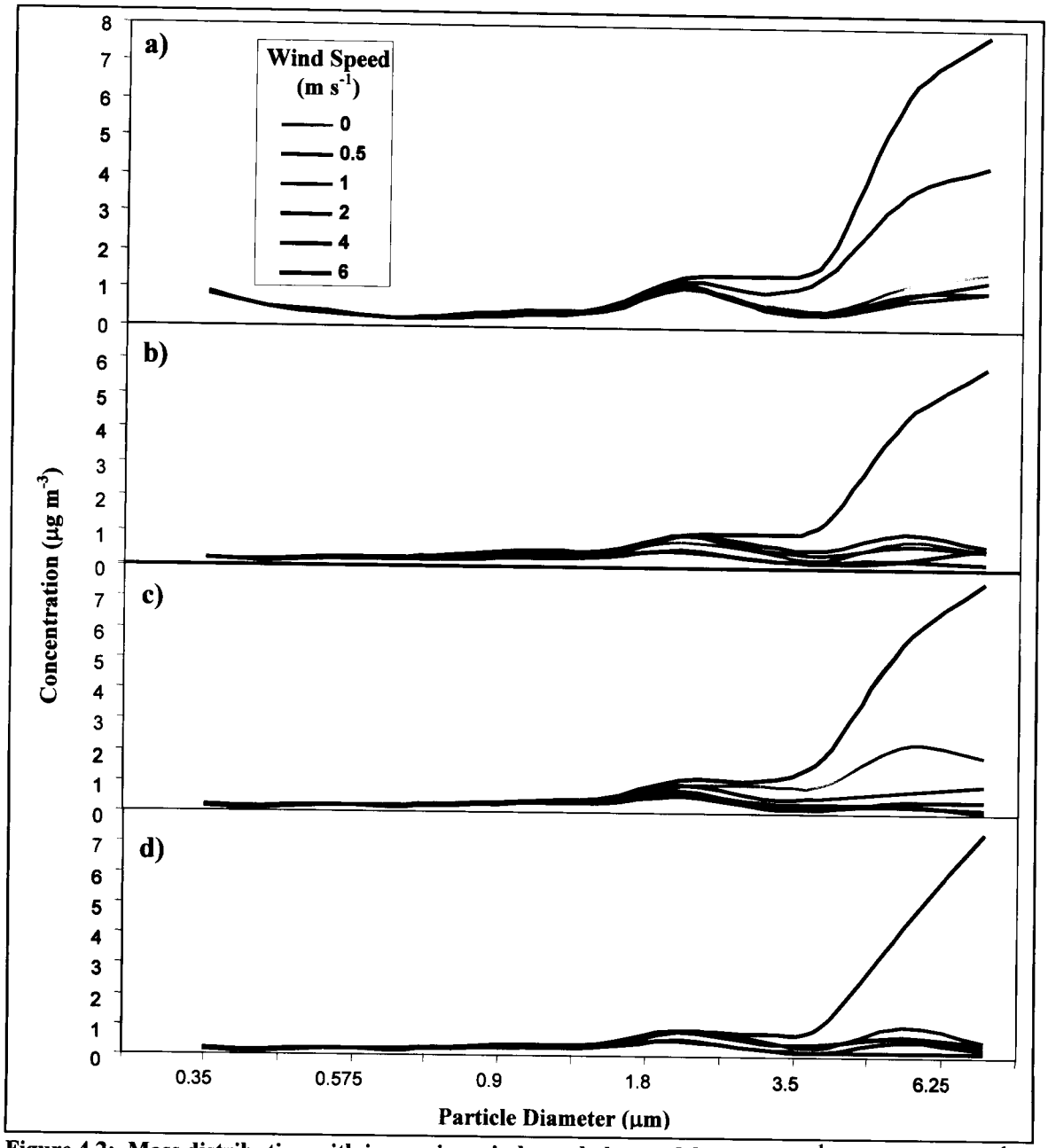

Figure 4.2: Mass distribution with increasing wind speed observed for (a) 4 $m\ s^{-1}$ intake, (b) 2 $m\ s^{-1}$ intake, (c) 1 $m\ s^{-1}$ intake, and (d) 0.5 $m\ s^{-1}$ intake.

Overall, the minor deviations between intakes suggested that the sampling ability of the GRIMM, for the wind speed range of interest, is not substantially affected by the choice of intake. Also, each intake appears suitable for use with a wind speed range of 0-6 m s^{-1}. As a precaution, it may be wisest to use the 4 m s^{-1} inlet during airborne measurements simply because it has a suitability approximately at the central point of the expected wind speed range.

4.3. Calibration Results

4.3.1. Gravimetric Comparison Between the GRIMM and a TEOM

As previously mentioned, GRIMM measurements of mass concentration are expected to deviate from true mass concentrations. To observe the magnitude of this error, the GRIMM was tested against a TEOM. A description of the TEOM is provided in the previous chapter. Figures 4.3a and 4.3b compare measurements of PM_{10} and $PM_{2.5}$, respectively, obtained with the GRIMM and TEOM. It is clear that the GRIMM consistently underestimates mass concentration. This systematic error is expected because the GRIMM is limited to particles greater than 0.3 μm. Figure 4.3c illustrates the PM_{10} comparison with the $PM_{2.5}$ deviation removed. As expected, the majority of the PM_{10} deviation occurs within the $PM_{2.5}$ component. The deviation is not, however, purely systematic as the trends are not identical. Concentrations for June 18 and July 3 show less deviation. Conditions for those two days were windy hence larger particles likely made up a larger proportion of the mass. Also, some error likely stems

from the GRIMM's use of a single density to estimate mass. GRIMM measurements therefore cannot be completely adjusted with a simple multiplication by a correction factor.

An adequate adjustment, however, can be performed by considering the mass signature for a given site during specific conditions as well as the density signature for that site. Since there is little variation in sources for a given site of small spatial extent, an average density for a given particle size-range can be used to modify the GRIMM output. This would indeed provide a more accurate result than relying on an average density for the entire range. Such density signatures have been widely studied in Southern California (Chow et al., 1992; Watson, 1994) and will be available for the LFV as a result of the Pacific 2001 Field Study. Mass signatures at a given site are likely to have greater variation. Specifically, they are likely to vary with day/night and calm/windy situations. These situations, however, provide standard enough mass signatures to allow simple calculation of correction factors suitable for a given condition. Once adjustments have been made for particle densities, correction factors may be calculated from a gravimetric instrument such as the TEOM.

Density signatures were not available during this research. Consequently, appropriate adjustments could not be made to GRIMM outputs. However, since the majority of the error appears systematic, it is assumed that results presented in the following chapters include a consistent negative deviation.

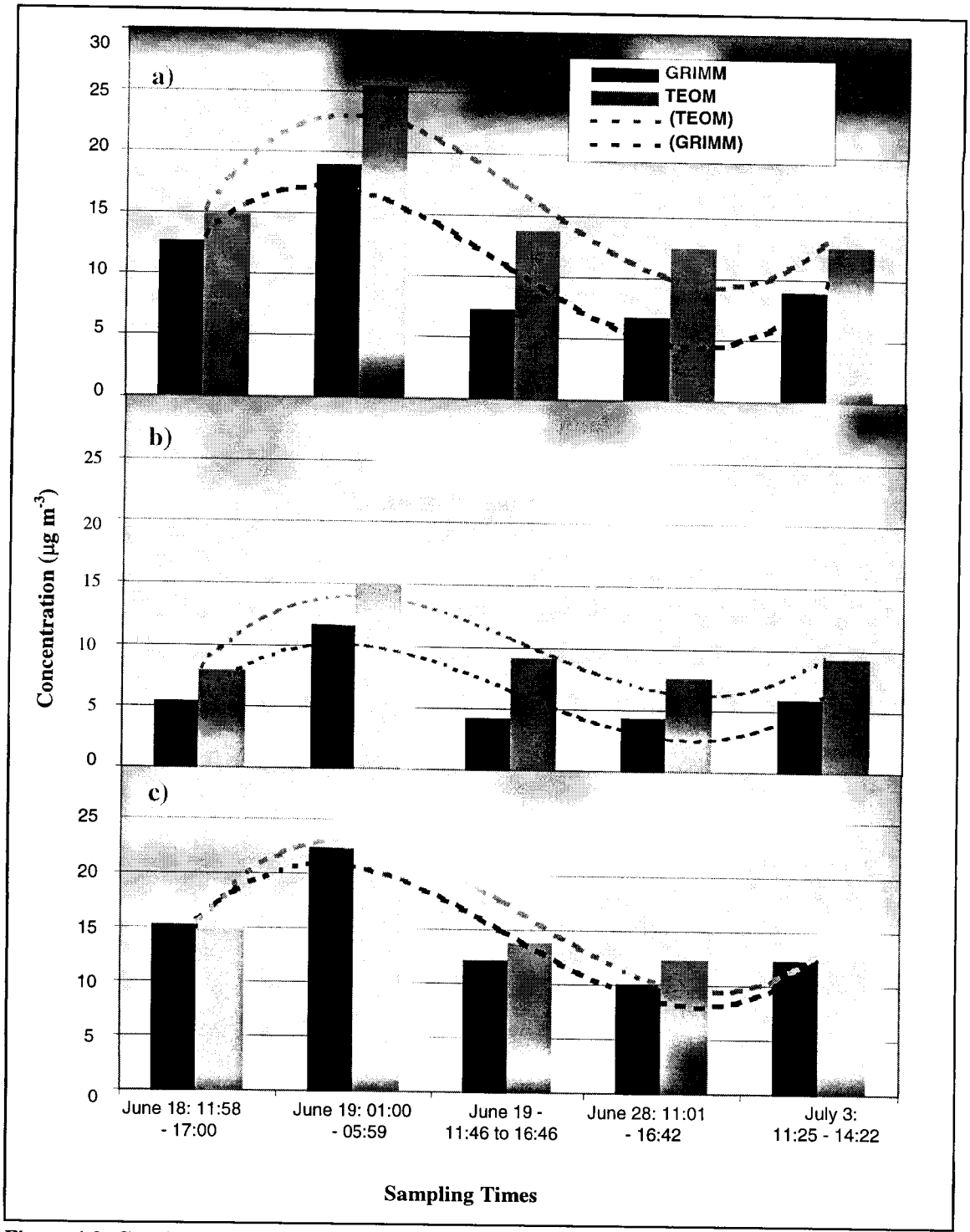

Figure 4.3: Gravimetric comparison of the GRIMM and a TEOM for (a) PM_{10}, (b) $PM_{2.5}$, and (c) adjusted PM_{10}. Trend lines are not statistically meaningful but are meant to be a visual aide.

4.3.2. Time Series Comparison Between the GRIMM and a PCASP

The GRIMM's temporal response characteristics are not specified clearly in the instrument manual. Consequently, it was necessary to compare a time series observed with the GRIMM to one observed with a calibrated instrument. Figure 4.4 compares a time series obtained with the GRIMM to one measured with a PCASP. A description of the PCASP is provided in the previous chapter. Although the two instruments provide eight particle bin sizes that overlap, only one could be used for comparison (the August 28 time series are not used as the intake was completely removed from the GRIMM). Time series for all other bins show extreme deviation that is likely caused by the PCASP's difficulty in sampling larger particles (Richard Leaitch, personal communication).

The PCASP particle count data were converted to mass concentration with the same two assumptions used by the GRIMM: (a) all particles are spherical and (b) all particles have an average density of 2 g m^{-3}. The two series clearly demonstrate that the GRIMM is a reliable instrument for taking real-time measurements. The consistent negative deviation from the PCASP series most likely results from the GRIMM's smaller bin range. The deviation between the two series would vary according to the concentration of particles not included in the GRIMM's bin. It can thus be concluded that, neglecting the above-mentioned systematic underestimate of mass concentration, the GRIMM should be capable of adequately measuring vertical profiles of particulate matter under conditions in which concentrations change rapidly with height.

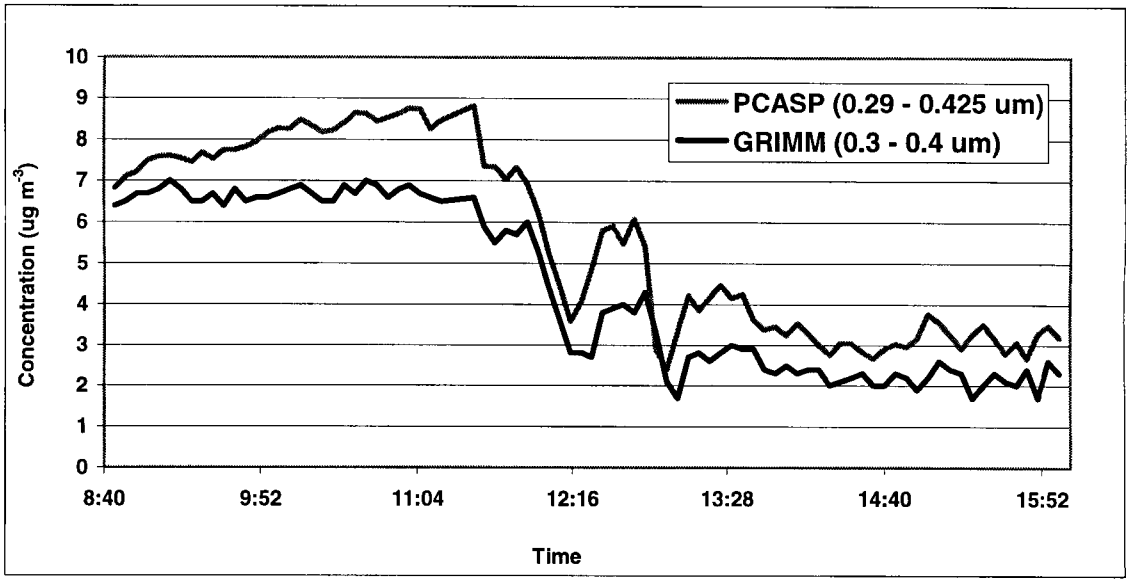

Figure 4.4: Time series comparison between the GRIMM and a PCASP.

4.4. Conclusion and Recommendations

The results presented in this chapter suggest that the GRIMM is suitable for measuring vertical profiles of particulate matter. Wind sensitivity tests propose that the instrument can measure within a wind speed range of 0-6 m s^{-1} with a single intake. However, the tests were performed with the assumption that the mass concentration of particulate matter within a closed room would remain relatively constant for a period of two days. The assumption proved to be incorrect even if changes in the mass concentration were minor. In addition; the 'cleansing' procedure used with the tunnel at the beginning of each day appears to have had no effect. Most likely, large particles entrained during maximum testing speeds settled out once the speed was reduced. Although these results are convincing, further testing of the GRIMM for wind sensitivity in a completely controlled environment is recommended.

Gravimetric comparison of the GRIMM with a TEOM shows that most of the error present

in GRIMM measurements likely results from its exclusion of particles with diameters less than 0.3 μm. Additional error may be due to oversimplification of ambient particle densities. These errors may be corrected with site-specific knowledge of particle size distribution and density signatures.

A time series comparison between the GRIMM and a PCASP demonstrates that the GRIMM is capable of taking accurate continuous real-time measurements. Hence, it should be able to observe representative vertical profiles. Unfortunately, the time series used is only for a single bin size. Although the good correlation may represent the GRIMM's ability to continuously measure for all its bin sizes, there is a possibility that it does not. The GRIMM may be more accurate for certain bins because it quantifies refraction based on a group of particles rather than a single particle at a time. Consequently, calibration should be performed against a calibrated instrument that can properly collect particles within the same size range as the GRIMM. This may actually prove to be difficult as many instruments that take size-segregated real time measurements appear to have difficulty collecting large particles or, if they capture large particles, they do not incorporate finer particles. It may thus be necessary to calibrate the GRIMM with two other instruments.

Overall, the results show the GRIMM to be suitable for deployment on a tethered balloon. Consequently, the instrument was used to measure vertical profiles during the Pacific 2001 Field Campaign. The following chapter presents two case studies that resulted from the field campaign.

Chapter V: Vertical Profiling using a GRIMM Particle Dust Monitor

5.1. Introduction

The Lower Fraser Valley (LFV), British Columbia is a coastal region with complex terrain. The valley floor is flat with low altitude while the surrounding mountains are steep and reach altitudes of 2000 m. The air pollution meteorology of the region is thus strongly influenced by local circulations including the land/sea breeze and valley/mountain winds (McKendry et al.,1998; Steyn and McKendry, 1988) as well as other processes described in Chapter 2. The majority of pollutants in the valley originate from the north-western edge, that is Greater Vancouver which has a rapidly growing population of nearly 2.0 million. The remainder of the valley is primarily rural with interspersed small urban centres.

While the meteorology, chemistry, and behaviour of gaseous pollutants in the LFV are reasonably well known, the PM_{10} meteorology of the region is less well understood. PM_{10} concentrations are relatively low by comparison to other urban centres such as Los Angeles, Toronto, Philadelphia, Birmingham (UK), and various other urban sites across Europe (McKendry, 2000). The LFV is seldom influenced by long-range transport of particulate matter (McKendry, 2000). Also, spatial variations in annual mean concentrations are relatively low (Figure 2.4). This suggests that LFV PM_{10} concentrations are primarily modulated by meteorological conditions and within-valley sources. McKendry (2000) identifies three main conditions responsible for particulate matter episodes in the LFV:

(a) short summer night time periods (1-3 hours duration) of reduced dispersion when winds are light or calm and a nocturnal boundary layer is present;

(b) summer daytime, anticyclonic conditions when winds are light and dispersion is reduced, and

(c) occasional wintertime "gap wind" events limited to the eastern part of the LFV and associated with the re-suspension of crustal material by strong winds.

As inother regions, vertical information on PM_{10} in the LFV is not available. Although the valley does not frequently experience elevated PM_{10} concentrations, its geography makes it a good location for studying complex air pollution meteorology. Consequently, the measurement of vertical profiles in the valley can greatly help in understanding PM_{10} meteorology in other similar regions. Profiles can help in explaining processes affecting the production, transport, and distribution of airborne particles. Specifically, profiles allow assessment of the diurnal evolution of mixing processes and determination of the signature of elevated pollution layers. Profiles also provide observations for the development and validation of air pollution models.

In this chapter, two case studies are presented to illustrate results arising from the measurement of PM_{10} vertical profiles in the LFV; the first at Pitt Meadows and the second at Langley. The Pitt Meadows study focuses primarily on the diurnal vertical evolution of PM_{10} while the Langley study examines an elevated pollution layer and Lidar validation. Both studies discuss the mass distribution of particles with altitude.

5.2 Pitt Meadows Case Study

5.2.1. Site Description

Pitt meadows is located at the entrance of a tributary valley in the northern portion of the LFV (See Figure 5.1). During summertime anticyclonic conditions, the site is susceptible to elevated pollution episodes. During the day, the combination of sea-breeze and mountain flow allow Vancouver's urban plume to reach the site and extend beyond it northward up the Pitt Lake tributary valley (McKendry et al. 1997). At night time, drainage winds exiting the Pitt Valley often contain aged pollutants originating from the Vancouver side of the LFV (Banta et al. 1997). The site itself is semi-rural but influenced locally by a major highway situated approximately 2 km to the south.

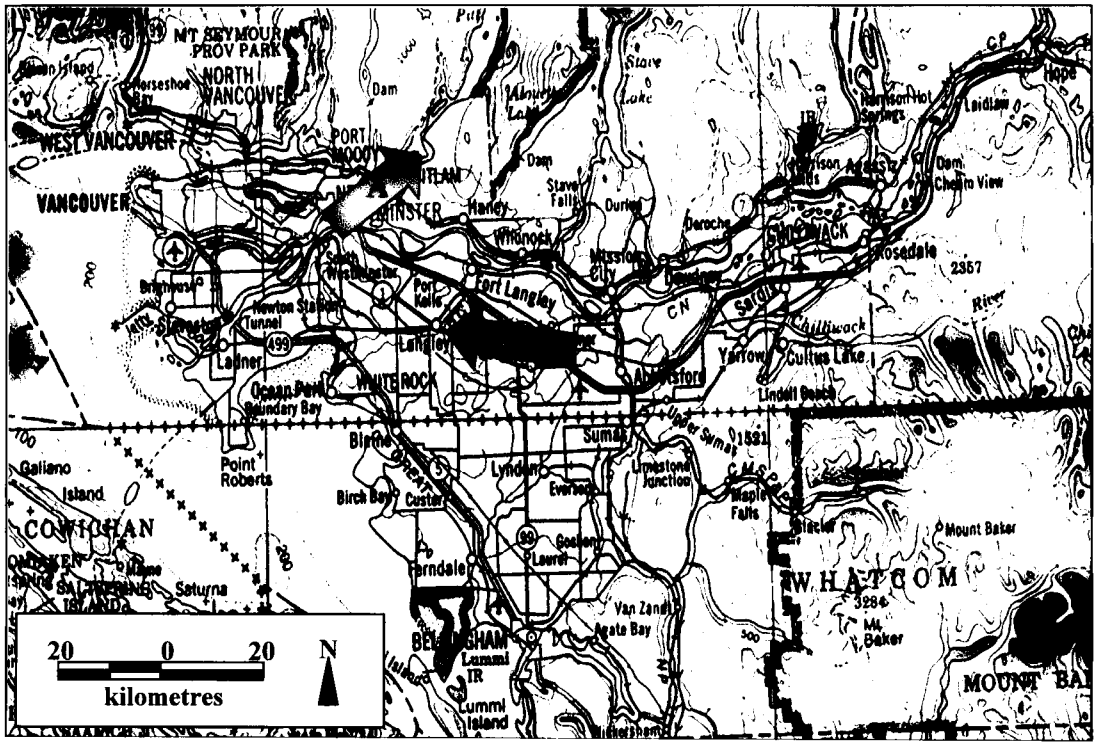

Figure 5.1: Map of the Lower Fraser Valley. A is Pitt Meadows and B is Langley Township.

5.2.2. Data Collection and analysis

Data were collected during 25, 26, and 27 July, 2001. A period of light rain in the region terminated two days before commencement of data collection. During the study period, anticyclonic conditions were present. These clear conditions ended in the mid-afternoon of July 27. For vertical profiling through the boundary layer, the GRIMM was suspended approximately 1m below a 5 m^{-3} helium filled tethered balloon (Figure 5.2 and Plate 2). In addition, an Atmospheric Instrumentation Research Inc. (AIR) Tethersonde (TS-3A-SPH) was suspended below the GRIMM in order to provide wind speed, wind direction, temperature, humidity, and pressure approximately every 10 seconds. Meteorological information was telemetered to a ground station while particulate matter data was recorded at 1-minute intervals on the GRIMM memory card. Ascent and descent of the balloon was controlled by an electric winch. A typical ascent/descent sequence reaching 1 km above the ground had a total duration of 70 minutes. This gave a vertical resolution for the meteorological data of 5 m and 28.5 m for the particulate matter data. The 5 m^3 tethered balloon proved sufficient for lifting the GRIMM and a meteorological package up to an altitude of approximately 1 km. However, the balloon required maximum inflation and lifting potential decreased rapidly with increasing wind speed.

The frequency of balloon launches depended mostly on time of day. Profiles were measured more frequently during rapidly changing boundary layer conditions, that is, the morning development of the boundary layer and evening establishment of the stable boundary layer. In all, 24 profiles were obtained during the study period (Table 5.1).

Date	Start Time*	Top Time	End Time	Max Height (m)
07/25	15:03	15:32	16:07	711
07/25	18:19	18:56	19:34	968
07/25	20:10	20:47	21:22	811
07/26	09:06	9:43	10:16	1017
07/26	10:21	11:01	11:45	1027
07/26	13:18	13:55	14:31	1014
07/26	14:48	15:25	16:01	811
07/26	20:10	20:32	20:49	600
07/26	22:45	23:11	23:38	713
07/27	01:04	01:31	01:59	737
07/27	03:25	03:59	04:44	1004
07/27	06:13	06:39	07:03	677

Table 5.1: Description of profiles observed at Pitt Meadows. *All times are PDT.

Pressure and temperature profiles allowed the determination of heights at which size distributions were measured with the GRIMM (clocks on both the meteorological package and the GRIMM were synchronised). A sufficient number of consecutive profiles were available throughout 26 and 27 July to allow an interpolated plot depicting the diurnal vertical evolution of PM_{10}, potential temperature, wind speed, and wind direction.. In addition; sufficient mid-day and evening profiles were available to plot average mass distributions with altitude. Examination of all these plots is presented in the next section.

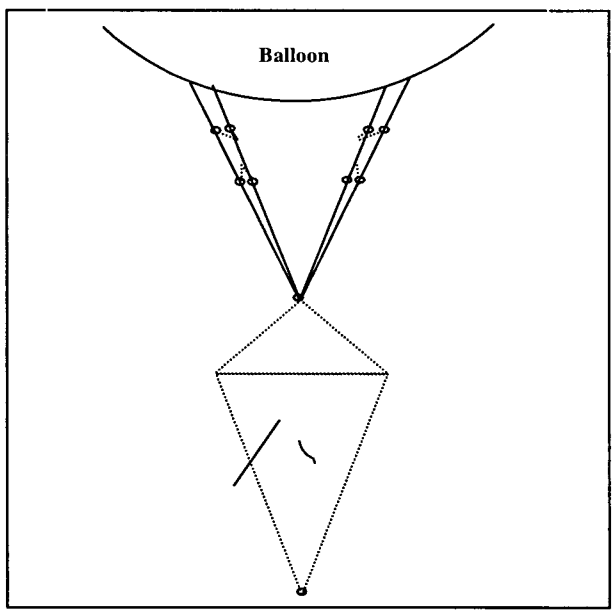

Figure 5.2: Schematic of instrument array during vertical profiling.

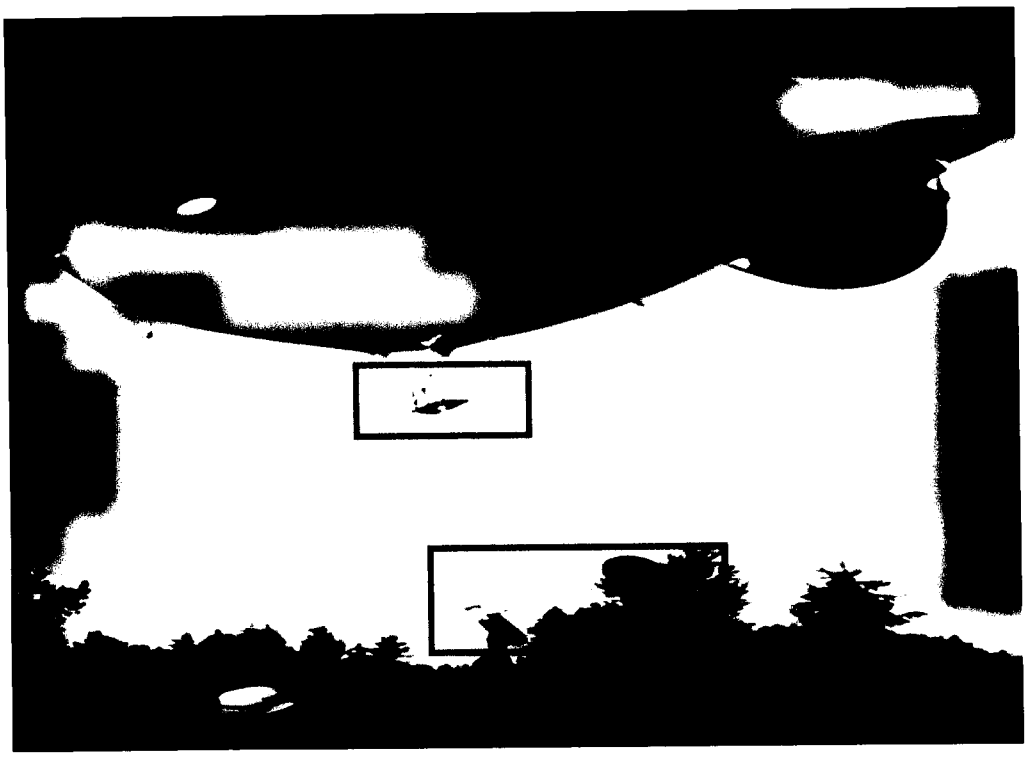

Plate 2: Instrument array.

5.2.3. Diurnal Evolution of Meteorological Variables and PM_{10}

. Observing the diurnal evolution (in the vertical) of meteorological variables and size-segregated particulate matter concentration can greatly help in understanding processes governing the vertical distribution of PM_{10}. This section examines such diurnal evolutions that occurred from July 26 to July 27, 2001.

Figure 5.3 illustrates the diurnal evolution of potential temperature, wind speed, and wind direction with height. The potential temperature contour plot helps determine the condition and height of the boundary layer. The wind speed plot also helps determine the height of the boundary layer, especially at night when a low-level jet is frequently established at the top of the stable boundary layer. As previously mentioned in Chapter 2, wind speed is sometimes positively correlated with increases in PM_{10} concentration hence the plot can also contribute to

explanation of temporal variations in concentration. The wind direction plot is used to detect flow directions and the origin of pollutants.

The beginning of the potential temperature plot shows the remainder of the previous night's stable boundary layer and the beginning of the daytime convective mixed layer. The mixed layer grows rapidly giving fully mixed conditions by 12:00 PDT (Pacific Daylight Time). The top of the mixed layer can be estimated by the presence of the temperature inversion. A combination of this plot and Lidar image for appropriate times (see Appendix II) place the mixed layer top at 750 m at 12:00 PDT and growing to its maximum of 800 m throughout the day.

The wind speed plot shows relatively calm conditions in early morning with wind speeds increasing with the development of the mixed layer. Wind speeds increase rapidly around 14:00 PDT and remain elevated throughout the day. This corresponds with the typical sea-breeze arrival time for this site (Douw Steyn, personal communication). The maximum speed occurs around 18:00 PDT and is followed by a steady decrease. Early morning wind is generally westerly and gradually changes to a southerly direction. Since some averaging occurs in interpolation, these flows suggest that early morning measurements were primarily detecting larger scale valley outflow rather than Pitt Valley outflow. The shift in direction in mid-morning should correspond to the beginning of up-valley flow (Pitt Valley). The arrival of the sea-breeze appears to establish the general south-westerly wind for the remainder of the day.

Figure 5.4a illustrates the diurnal vertical evolution of PM_{10}. On the morning of July 26, the remaining night time elevated concentrations, and probable early morning

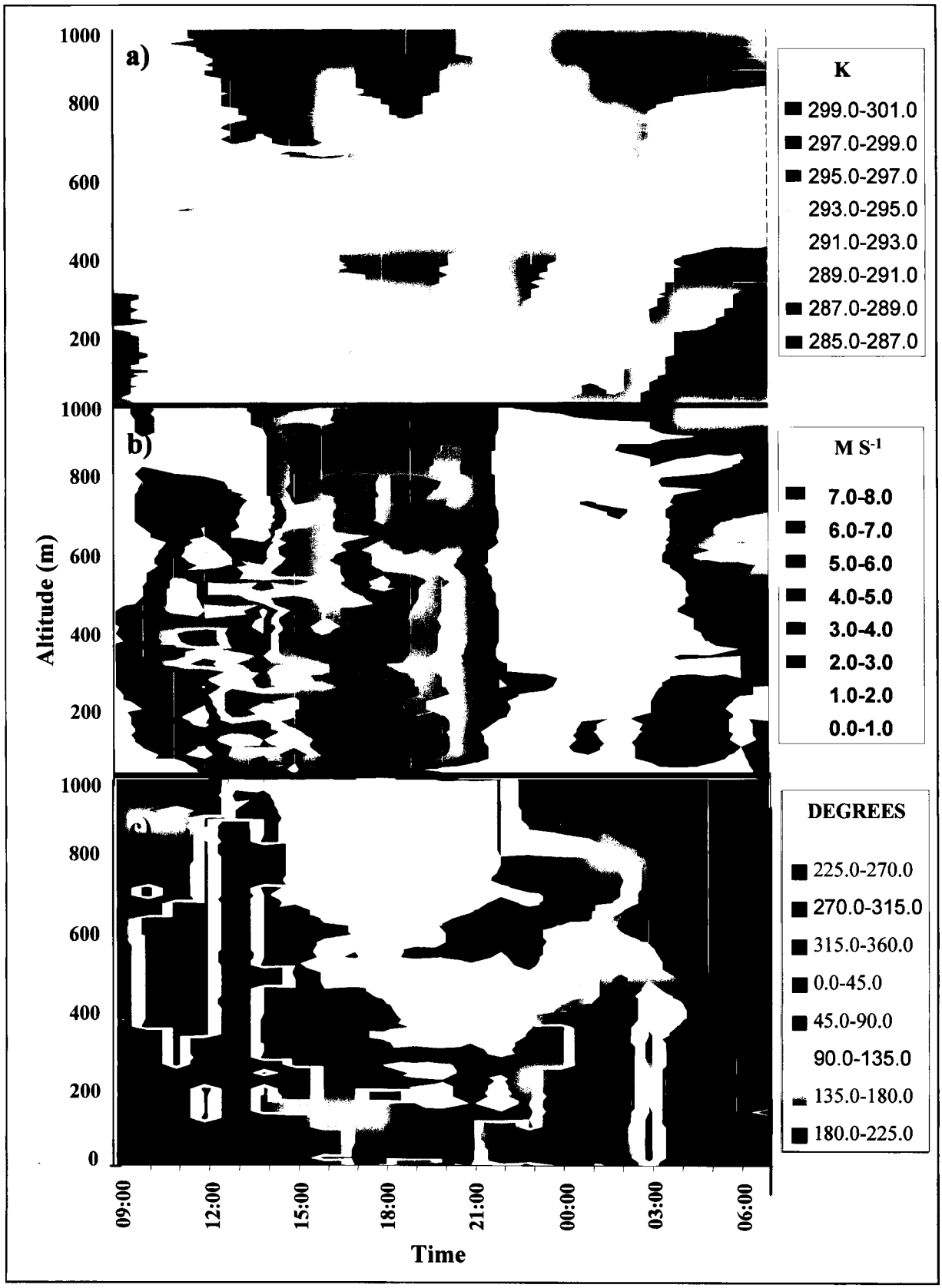

Figure 5.3: Diurnal evolution in the vertical of (a) potential temperature, (b) wind speed, and (c) wind Direction.

high concentrations from traffic hour, is diluted as the convective mixed layer grows. PM_{10} appears relatively well mixed from 12:00 PDT to 16:00 PDT. Surface concentration increase begins at approximately 16:00 PDT, corresponding to a surface decrease in wind speed. The pollution increase at the surface may be caused by a combination of reduced dispersion near the surface, increased local sources due to afternoon traffic hour, and accumulation of pollutants arriving with the sea-breeze. The very layered concentrations during mid-day is somewhat puzzling, however, it may be that the early breakdown of the convective mixed layer is responsible for the pollutants remaining unmixed.

The convective mixed layer appears to break down at approximately 18:00 PDT yet conditions appear to remain neutral until approximately 20:00 PDT. The mixed layer breakdown is accompanied by a rapid drop in wind speed below 100 m with near surface values of near 0 m s^{-1}. The lack of mechanical and free turbulence may allow for the surface accumulation to continue while winds of 6 m s^{-1} above 100 m seem to 'clean out' the upper levels.

The potential temperature plot shows the onset of a stable boundary layer at approximately 20:00 PDT. The stable boundary layer grows to a maximum of 400 m throughout the night. Surface winds remain at 0 m s^{-1} near the surface. These calm conditions extend in altitude until the development of a low-level jet. The absence of wind renders the corresponding portion of the wind direction plot invalid. The first appearance of a low-level jet is brief around 01:00 PDT. It appears to collapse and to re-establish itself at 03:00 PDT where it continues (roughly) with an increasing altitude until early morning. The direction appears to correspond to general valley outflow.

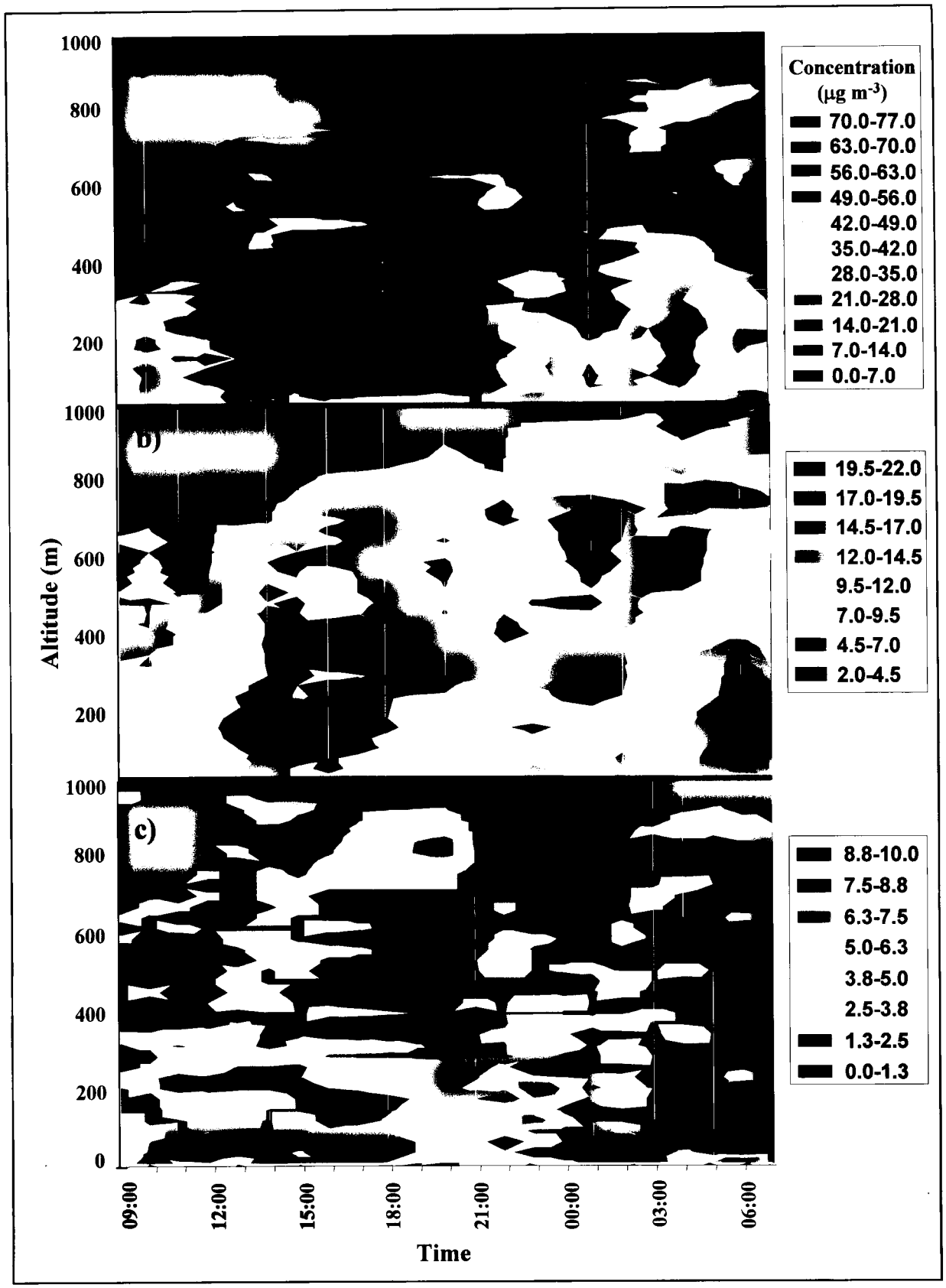

Figure 5.4: Diurnal evolution in the vertical of (a) PM_{10} , (b) PM_2 , and (c) $PM_{7.5-10}$

Night time boundary layer conditions provide a rational explanation for the PM_{10} behaviour observed. The shallow nocturnal boundary layer reduces dilution potential hence allowing concentrations to increase rapidly. In addition; calm conditions give a very low dispersion potential. It can therefore be assumed that all the pollution seen here originates from local sources. The concentrations observed for PM_{10} are much higher than the seasonal average of the valley (approximately 15 $\mu g\ m^{-3}$). The strongly stable atmosphere suppresses any free turbulence while calm conditions produce no mechanical turbulence. The result is a very stratified vertical distribution of PM_{10}. This stratification appears to be disrupted during the collapse of the low-level jet. This is likely due to intermittent turbulence caused by the low-level jet (the jet causes itself to collapse). However, once the low-level jet has strongly established itself, concentrations increase to their highest values of the 24-hour period.

It should also be noted that after 03:00 PDT, a shift in wind direction occurred between approximately 500 m and 800 m. This shift is above the low-level jet and corresponds to the appearance of an elevated pollution layer. This layer represents flow out of Pitt Valley and may be composed of pollutants transported up Pitt valley during the day. Elevated layers are discussed in more detail with the Langley case study.

Although the PM_{10} plot illustrates well-mixed conditions for the pollutant during the day, segregating the plot according to particle size shows that all size categories of PM_{10} do not behave homogeneously. Figure 5.4b and 5.4c illustrate the same temporal evolution as above but for PM_2 and $PM_{7.5\text{-}10}$ respectively. Smaller particles have a much smoother evolution displaying behaviour very analogous to gaseous pollutants (although not photochemical). There is obvious morning dilution, well mixed conditions during the mid-day, accumulation during

traffic hour, and the development of a sharp gradient during the strongly stable nocturnal boundary layer.

By contrast, the larger particles display a very 'patchy' temporal evolution. Most larger particles appear below 500 m yet, even within this small bin range, they do not appear well mixed. This likely results from variations in particle shape and density which subsequently affect terminal velocity. Such particle characteristics should perhaps be given greater consideration when particles are too large to behave as a gas. It should be noted that the large particles appear to comprise an equal amount of the night time elevated layer as the smaller particles. In addition; there is a significant elevated layer of large particles during the day. The presence of both these elevated layers suggest that, although most large particles exist within the lower 500 m of the boundary layer, they are in fact affected by processes creating elevated layers.

5.2.4. Mass distribution with altitude

The heterogeneous behaviour of the different size classes making up PM_{10} is also evident when mass distributions at different altitudes are compared. In the day (Figure 5.5a), the concentration of particles greater than 2 μm decreases constantly with height. This gradual decrease suggests that particles of this size range are settled out by gravity. Particles with diameters of 0.4 to 2 μm are thoroughly mixed throughout the PBL while those ranging from 0.3 to 0.4 μm show a slightly increasing concentration with height. The slight increase in concentration of the smallest bin range may be correlated to an increase UV with altitude allowing for more gas-to-particle conversion. The only exception to these overall trends is in the 800 m distribution, which is actually above the PBL.

Night time mass distributions (Figure 5.5b) show a negative correlation between concentration and altitude (up to 600 m) for all particle sizes. Here, a very stable boundary layer limits the already weak mechanical turbulence (very calm conditions) and causes the stratification of pollutants. At 700 and 800 m, high concentrations from the elevated layer are incorporated in the averaging. The mass signature aloft has a dominant mode at 2.5 μm rather than 8 μm, as observed near the surface. Although concentrations around 8 μm appear similar to those during the day, the dilution potential has decreased hence emissions of coarse particles are probably lower at night (due to calm conditions). By contrast, emissions of finer particles have perhaps remained the same allowing for an increase in concentration in a reduced volume.

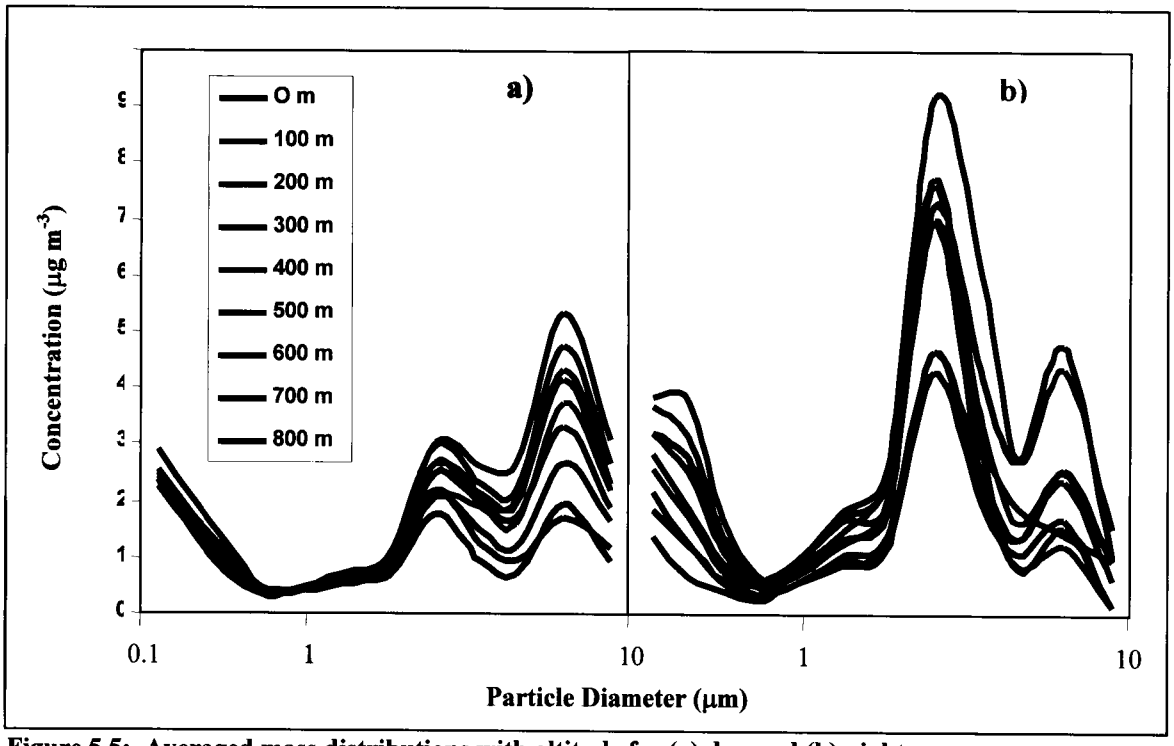

Figure 5.5: Averaged mass distributions with altitude for (a) day and (b) night.

The tri-modal signatures observed agree with signatures observed at similar sites i.e. traffic/urban-influenced sites with semi-rural surroundings. Modes at 0.2 and 2.5/3.0 μm are common for traffic/urban-influenced sites (Hidy, 1975; LeCanut et al., 1996; Morawska et al., 1998; Shi, 2001). A mode appearing at 8.0 μm for a site with semi-rural surroundings has also been observed by Hidy (1975). Although the signatures presented here are limited to particles with diameters greater than 0.3 μm, it is clear that a mode is present near the 0.3 μm cut-off.

When combining these results with those of the previous section, it is apparent that PM_{10} does indeed behave in a heterogeneous manner. Smaller particles become well mixed while larger particles remain at lower altitudes. The mass concentration of the residual boundary layers, which are re-entrained into the convective mixed layer, therefore have a greater proportion of smaller particles. This suggests that smaller particles are more prone to re-circulation than larger particles. As previously mentioned, however, larger particles make up a significant proportion of the two elevated layers observed at this site. Elevated layers may also be re-entrained into the convective mixed layer. Larger particles are therefore not immune to re-circulation. The following section describes the Langley case study which examines an elevated layer more closely.

5.3. Langley Case Study

5.3.1. Site description

Langley Township is located in the north-western section of the LFV (Figure 5.1), however, it has a more central location than Pitt Meadows. The area is reached by the sea-breeze during the day and affected by general valley outflow during the night. The site itself is

semi-rural but influenced locally by the small urban centre of Langley City and under northwesterly winds by the urban plume of greater Vancouver.

5.3.2. Data Collection and Analysis

Intensive observations were made on 9, 10, 11, 14, and 15 August, 2001. During the entire study period, and for the days surrounding, anticyclonic conditions were present. Vertical profiling through the boundary layer was obtained using an instrument array identical to that used at Pitt Meadows. A typical ascent/descent sequence reaching 700 m (the maximum altitude permitted by Nav Canada for this site) above the ground had a total duration of 45 minutes. This gave a vertical resolution for the meteorological data of 5 m and 28.5 m for the particulate matter data.

The frequency of balloon launches depended, again, mostly on time of day with a succession of profiles being measured during rapidly changing boundary layer conditions. In all, 56 profiles were obtained during the study period although four profiles were discarded due to instrumentation and lift problems (Table 5.2). In fact, lift was much more problematic during this study. Cold temperatures at night quickly reduced the lifting potential of the balloon. In addition, rupturing problems began to occur with the balloons. This may have been caused by the over-inflation necessary to lift the combined instrument payload.

Date	Start Time*	Top Time	End Time	Max Height (m)
08/09	08:53	09:10	09:27	343
08/10	14:22	14:41	14:56	743
08/10	05:23	05:43	06:10	266
08/10	06:38	07:07	07:22	524
08/10	08:51	09:07	09:22	747
08/10	10:52	11:09	11:25	760
08/10	15:10	15:30	15:47	742
08/10	17:06	17:26	17:47	701
08/10	20:05	20:26	20:45	744
08/10	21:13	21:30	21:49	446
08/11	22:18	22:38	22:55	756
08/11	00:02	00:17	00:32	691
08/11	04:13	04:33	04:47	586
08/11	05:24	05:41	05:58	731
08/14	06:18	06:37	06:54	745
08/14	16:05	16:22	16:37	612
08/14	17:49	18:08	18:25	758
08/15	19:15	19:32	19:55	701
08/15	05:33	05:39	05:47	116
08/15	06:22	06:39	06:54	693
08/15	07:37	08:01	08:22	727
08/15	09:15	09:36	09:57	705
08/15	15:23	15:47	16:09	765
08/15	17:50	18:06	18:21	582
08/15	19:30	19:49	20:07	625
08/15	20:39	21:00	21:20	609

Table 5.2: Description of profiles observed at Langley Township.

Although more profiles were obtained than at Pitt Meadows, emphasis is placed here on selected mid-day averaged mass distributions with altitude, the mass distribution signature of an elevated layer (observed on August 15), and comparative plots of GRIMM and Lidar output. All of these plots are presented in the following section.

5.3.3. Validation of GRIMM observations using Lidar

Although Lidar cannot be used to calibrate the GRIMM, it is useful in validating

observations. The Lidar name refers to light direction and ranging system or laser radar. The laser component transmits a short and intense pulse of light that is expanded to minimize its divergence, and is directed by a tiltable mirror into the atmosphere. As the pulse travels it is scattered by atmospheric gases and aerosol particulates. Light that is backscattered and in the field-of-view of a telescope receiver is collected and channelled toward a detector. Because particulate matter causes scattering, Lidar can be used to detect its relative concentration in the atmosphere. This relative value can provide a good qualitative assessment of particulate matter present. Figure 5.6 shows three comparisons of Lidar images with vertical profiles obtained with the GRIMM. In essence, these images demonstrate the GRIMM's ability to detect sudden or gradual changes in concentration while in motion. All simultaneous Lidar and GRIMM observations obtained during either field study show good agreement (see Appendix II).

Lidar imagery provides a good qualitative assessment of pollution the PBL and is extremely valuable in detecting elevated pollution layers. The lack of quantitative information, however, makes it difficult to determine the origin of the layer. *In situ* measurements can provide mass distribution signatures that can aide in determining the origin of a layer. Such measurements alone, however, often cannot distinguish between the presence of a true layer and a pocket of polluted air. This is especially true for vertical measurements taken at a single horizontal point. Lidar images and vertical profiles can thus be used in combination to provide more informative results. Vertical profiles of particulate matter and meteorological variables, in turn, complement the qualitative information provided by a Lidar. Size-segregated PM_{10} profiles can provide the mass concentration and mass signature of elevated layers. An example of these combined methods is presented in the following section.

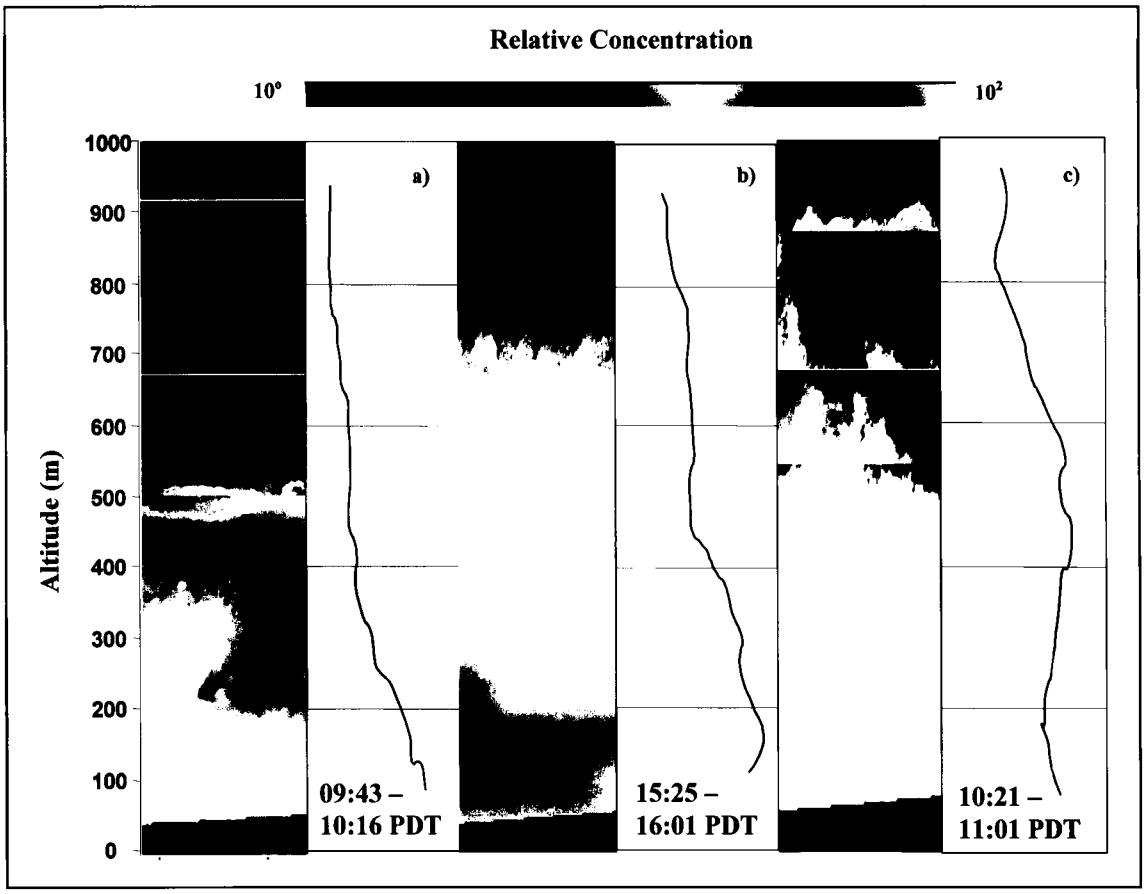

Figure 5.6: Comparison of Lidar images with vertical profiles obtained simultaneously with the GRIMM. Three comparisons are shown from July 26 with (a) showing detection of gradual changes, (b) detection of minor abrupt changes, and (c) detection of major abrupt changes.

5.3.4. An early evening elevated pollution layer

Elevated pollution layers are of substantial interest in air pollution meteorology because of their potential to be entrained into a convective mixed layer and consequently affect surface concentrations. As mentioned above, the presence, composition, and origin of mixed layers may be difficult to determine. Figure 5.7b shows a vertical profile obtained with the GRIMM. A significant increase in concentration occurs above 300 m. This increase may be attributed to an elevated layer but it is difficult to confirm without taking simultaneous profiles or without a

Lidar image. Figure 5.7a shows a Lidar image taken at the same location and time as the profile. The image clearly confirms the presence of an elevated layer and therefore supplements the information that can be extracted from that single profile.

The layer appeared around 21:00 PDT, after the onset of the nocturnal boundary layer and the beginning of a low-level jet at approximately (Figure 5.8). Figure 5.7c compares the signature of the elevated layer to that of the stable boundary layer. The two are plainly different with the elevated layer having a signature similar to a daytime ground-level signature found at the Langley site (Figure 5.9) and at the Pitt Meadows site (Figure 5.5a). The meteorological profiles also show the presence of 'different' air in this region of the profile. There is a considerable increase in specific humidity and wind speed as well as an 180^{o} change in wind direction. Such characteristics of the layer help to isolate it from the surrounding air and may in fact aide in determining the layer's origin. Unfortunately, wind direction at this site varies enormously from day to day and within the day. Consequently, the wind profile does not represent the reverse of daytime conditions. It is therefore difficult to estimate where the layer may have originated, particularly since the layer's signature may be a common near surface signature.

As with the elevated layers observed at Pitt Meadows, a substantial proportion of this layer's mass concentration stems from large particles. This is yet more evidence that large particles are affected by processes creating such layers. It is unlikely, however, that convective penetration and/or cloud venting are responsible for elevating large particles considering the pattern illustrated by day time mass distributions with altitude. Since the layer has a ground-level signature, it is more likely to have been advected near the ground and elevated via mountain venting. This would allow the signature to remain the same since altitude is changing

altitude is changing but the height above ground is not. Once vented above the boundary layer, particles should be less affected by gravity, allowing the layer's composition to remain intact.

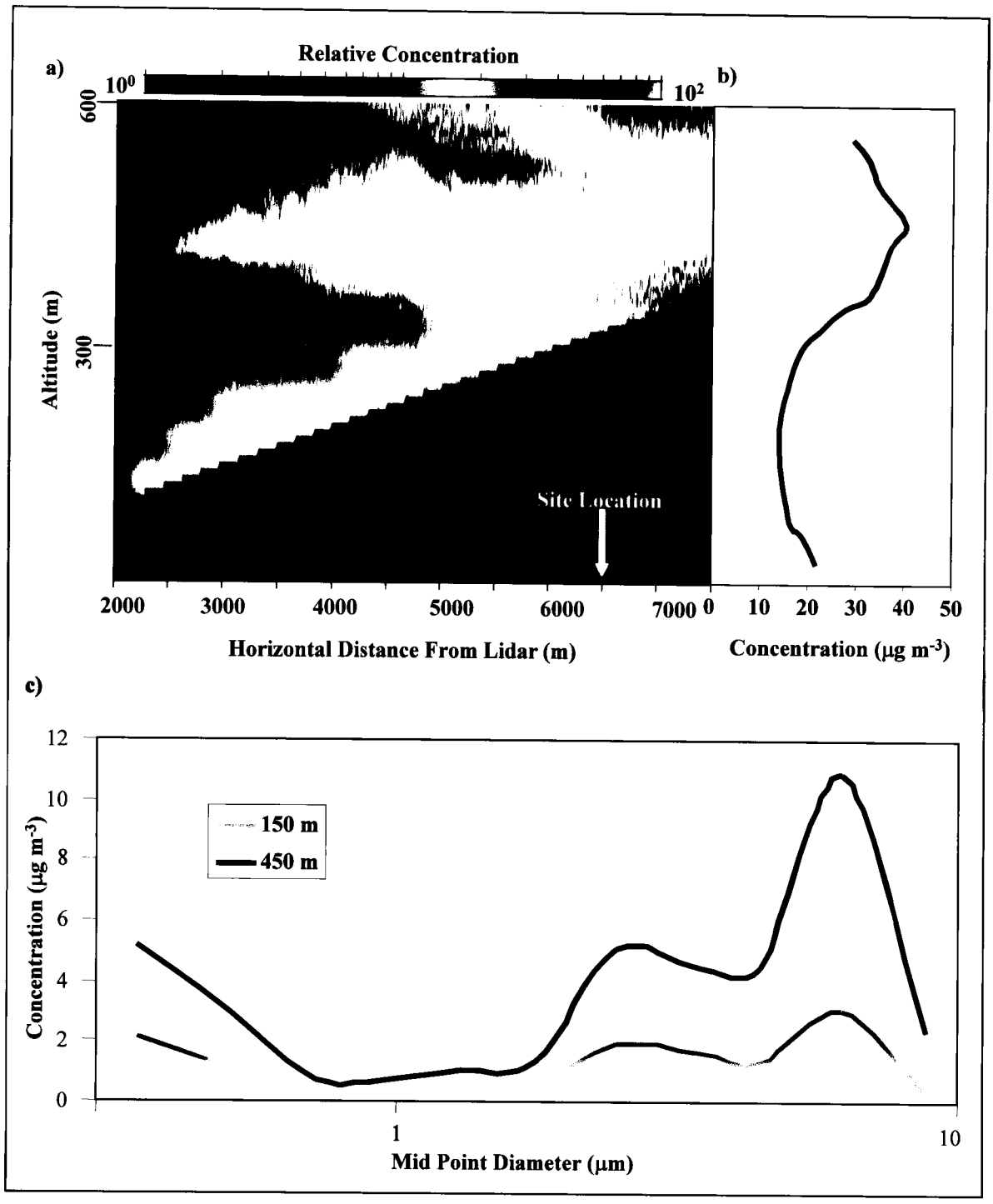

Figure 5.7: Detection of an elevated pollution layer on August 15 with (a) Lidar and (b) GRIMM. The mass distribution signature of the layer is compared to that of the surface in (c).

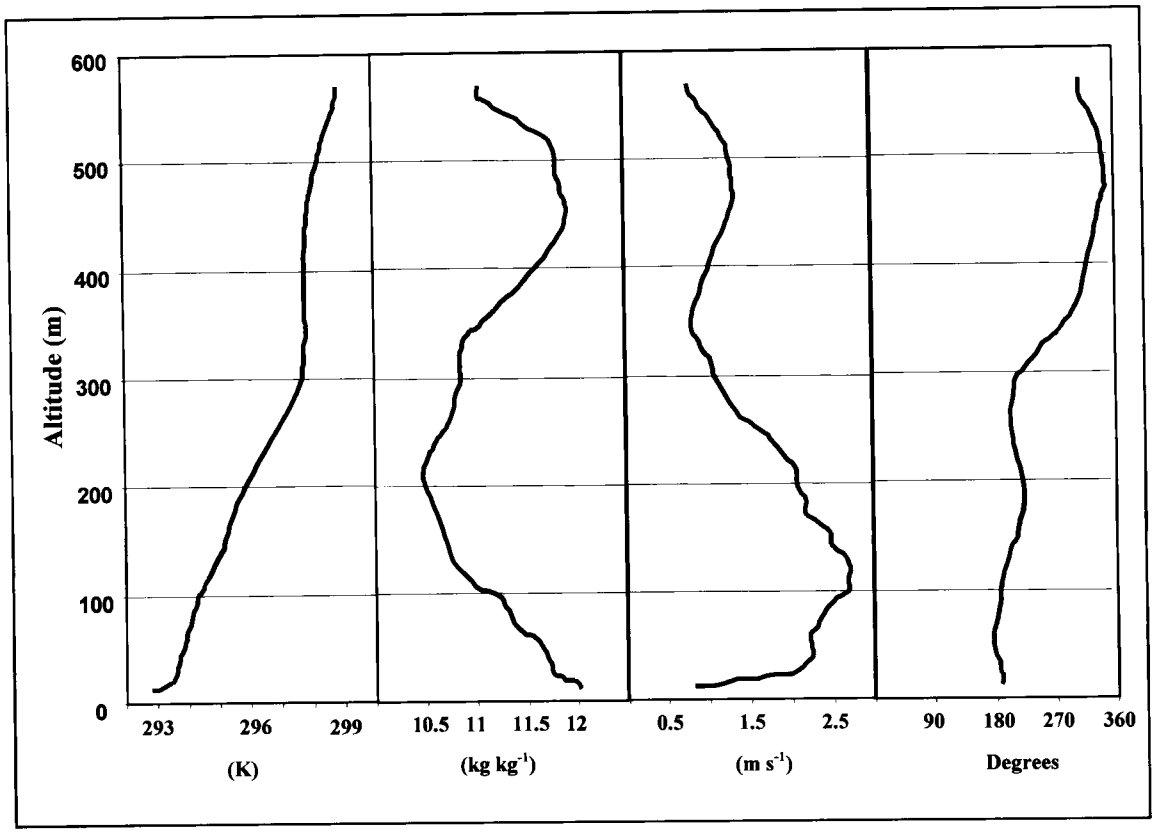

Figure 5.8: Vertical profiles of (a) potential temperature, (b) specific humidity, (c) wind speed, and (d) wind direction obtained during passage of the elevated pollution layer taken on August 15 between 21:00 an 21:20 PDT.

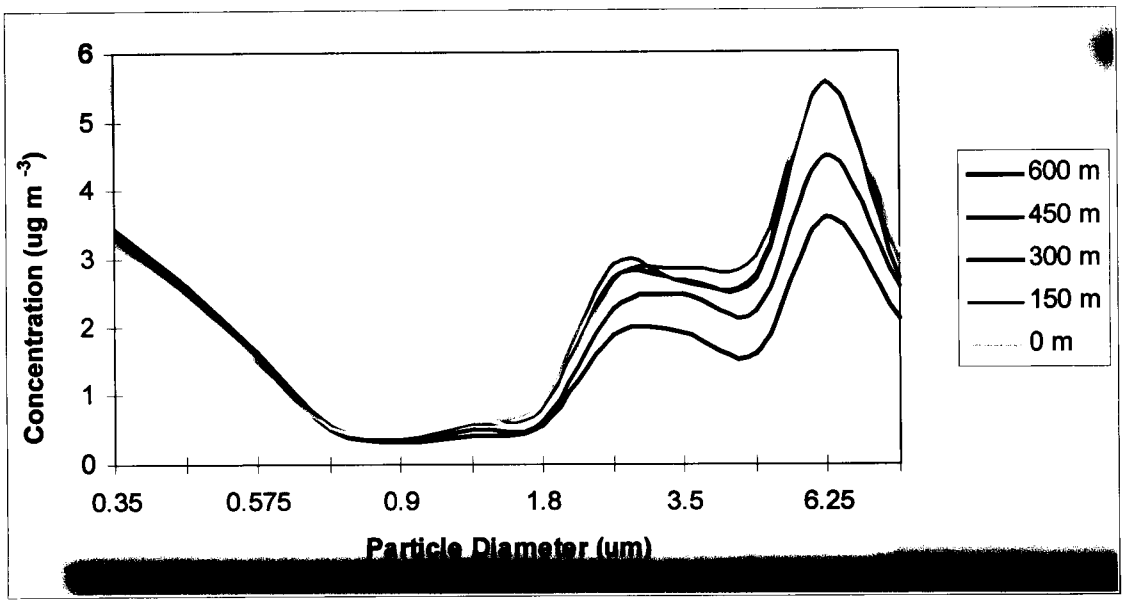

Figure 5.9: Averaged mass distribution with altitude during mid-day for August 15.

Combining Lidar imagery, meteorological profiles, and PM_{10} profiles provides a powerful set of tools for examining elevated pollution layers. Although further research would be required to make generalizations, the elevated layers observed in this research appear to have qualities analogous to near-surface air. Much more in depth and extensive observations would be required, however, to determine the origin of layers.

5.4. Conclusions and recommendations

The two case studies presented in this chapter provide a considerable amount of information about the vertical distribution of PM_{10}. The Pitt Meadows case study provides a good overview of the type of vertical distribution expected throughout a 24-hour period during anticyclonic conditions. It also provides some explanation for the variation in surface concentrations throughout a 24-hour period. From a data collection perspective, however, future profiles should be obtained at the maximum frequency possible to reduce the amount of interpolation required to create contour plots. Also, it may be preferable to use a slightly bigger tethered balloon to avoid both lift problems and damage caused by over-inflation.

The mass distributions with height provide evidence that PM_{10} does in fact behave heterogeneously in the vertical, with large particles settling out faster than smaller particles which become well-mixed. By contrast, all the elevated pollution layers observed show the presence of large particles. Considering the reduced level of upmixing of these large particles, mountain venting is suggested as the most probable mechanism responsible for their presence aloft.

All of these findings enhance the present state of knowledge of PM_{10}, however, their limitations should be considered. The findings result from two case studies and thus cannot be used to infer generalizations about the vertical behaviour of PM_{10}. In addition; the data are not calibrated due to lack of information at these study sites. Although a systematic underestimate of mass concentration is assumed, additional error is likely to be present and must be corrected. Comparison of the profiles obtained with simultaneous Lidar images provides good qualitative validation for the results but this is not enough to ensure complete confidence.

The overall results of this chapter do demonstrate promise for future research. Multiple, simultaneous profiles of PM_{10} and meteorological variables can be measured and combined with Lidar imagery. Such a field campaign is reasonable, considering the relatively low cost of the GRIMM, and would provide extensive information for model development and validation. Results could also be used to attempt the development of algorithms that would convert Lidar output to mass concentrations. This would greatly facilitate three-dimensional measurements and improve knowledge of PM_{10} meteorology.

Chapter VI: Summary and Conclusions

Current research of other air pollutants suggests that the present knowledge of PM_{10} is not adequate for the development of dispersion models. These studies show that pollution dispersion is controlled by a complex combination of processes and that, to properly understand these, observations must be made in three dimensions. This is especially true in coastal regions with complex terrain, such as the LFV, where land/sea-breeze cells and mountain/valley wind circulations produce intricate three-dimensional distributions of pollutants. An adequate understanding of the vertical distribution is especially important for this pollutant because its chemical and physical composition is not homogeneous.

In this thesis, an attempt is made to remedy this significant research gap by describing the novel deployment of a miniature particle spectrometer (GRIMM Particle Dust Monitor 1.108) on a tethered balloon. Concerns about the instruments ability to measure vertical profiles were first addressed. Of greatest concern was the GRIMM's sensitivity to varying wind speeds. Consequently, wind tunnel tests were performed to determine whether or not the GRIMM could accurately measure mass concentrations within a wind speed range expected during deployment on a tethered balloon. The results propose that the instrument is in fact suitable for such a wind speed range. However, some assumptions made regarding the control of the testing environment proved to be incorrect. It is thus recommended, for future research, that tests be performed in a truly controlled environment if full confidence in the instruments appropriateness is to be achieved.

In addition to wind sensitivity testing, the GRIMM required calibration for three main reasons: (1) it does not measure particles with diameters smaller than 0.3 μm thus neglecting a substantial portion of the mass concentration, (2) it uses a single density to estimate mass causing its output to deviate from the true mass concentration, and (3) its ability to take independent real-time measurements is unclear. To address these problems, gravimetric comparisons were made with a TEOM and time series comparisons were made with a PCASP. The results from these comparisons suggested that negative systematic error is present in GRIMM output and that it likely accounts for the majority of the error encountered with this instrument. The results also indicated that the GRIMM is capable of taking accurate real-time measurements.

Overall, the results show the GRIMM to be suitable for deployment on a tethered balloon. Consequently, the instrument was used to measure vertical profiles during two field campaigns, one of which was incorporated in the Pacific 2001 Field Study. The two resulting case studies presented provide a considerable amount of information about the vertical distribution of PM_{10}. These give a good overview of temporal variations in vertical distribution and in surface concentrations throughout a 24-hour period. More importantly, evidence that PM_{10} does in fact behave heterogeneously in the vertical is provided. Upmixing of large particles appears to be limited causing the majority of their concentration to occur below 500 m above the surface. Small particles, by contrast, appear to become well mixed in a manner analogous to gaseous pollutants. These findings have significant implications for future model development as they suggest that PM_{10} should be modelled in parts rather than as a whole .

Elevated pollution layers were also observed and examined during both case studies. The observations demonstrate that large particles are indeed present in significant concentrations

within the particle composition of elevated layers. This result was not expected, especially after observing the limited amount of large particles found at higher elevations. Because a limited amount of large particle upmixing was observed, mountain venting is suggested as the possible mechanism responsible for elevated layers containing surface mass distribution signatures.

All of these findings enhance the present state of knowledge of PM_{10}, however, their limitations should be considered. Generalisations about the vertical behaviour of PM_{10} cannot be extracted from this research due to the nature of the observations and uncalibrated data. Comparison of the profiles obtained with simultaneous Lidar images provide good qualitative validation for the results but this is not enough to ensure complete confidence. This research, however, does offer promise for future PM_{10} research. Multiple, simultaneous profiles of PM_{10} and meteorological variables can be measured and combined with Lidar imagery to develop algorithms to extract improved size related information from Lidar which is limited to a 1 μm size range. Such a field campaign is reasonable, considering the relatively low cost of the GRIMM, and would provide extensive information for model development and validation. Subsequently, the development of accurate PM_{10} models can help to advance efficient emission abatement strategies.

References

Arya, S. Pal. (1999). Air Pollution Meteorology and Dispersion, Oxford: Oxford University Press.

Ayers, G.P., Keywood, M.D., Gras, J.L. (1999). TEOM vs. manual gravimetric methods for determination of PM2.5 aerosol mass concentration. *Atmospheric Environment*, 33, 3717-3721.

Banta, Robert M., Shepson, Paul B., Bottenheim, Jan W., Anlauf, Kurt G., Wiebe, H.A., Gallant, A., Biessenthal, T., Oliver, Lisa D., Zhu, Cui-Juan, McKendry, Ian G., Stey, Douw G. (1997). Nocturnal cleansing flows in a tributary valley. *Atmospheric Environment*, 31, 2147-2162.

Berico, M., Luciani, A., Formignani, M. (1997). Atmospheric aerosol in an urban area - measurements of TSP and of PM10 standards and pulmonary deposition assessments. *Atmospheric Environment*, 33, 3659-3665.

Blanchard, Charles L., Carr, Edward L., Collins, John F., Smith, Ted B., Lehrman, Donald E., Micheals, Harvey M. (1999). Spatial representativeness and scales of transport during the 1995 integrated monitoring study in California's San Joaquin Valley. *Atmospheric Environment*, 33, 4775-4786.

Chow, J.C. (1994). A laboratory resuspension chamber to measure fugitive dust size distributions and chemical compositions. *Atmospheric Environment*, 28, 3463-3481.

Chow, J.C., Watson, J.G., Lowenthal, Douglas H., Solomon, Paul A., Magliano, Karen L., Ziman, Steven D., Richards, L. Willard. (1992). PM10 source apportionment in California's San Joaquin Valley. *Atmospheric Environment*, 26A, 3335-3354.

Clark, A.G., Azadi-Boogar, G.A., Andrews, G.E. (1999). Particle size and chemical composition of urban aerosols. *The Science of the Total Environment*, 235, 15-24.

Colby, B.R. (1963). Fluvial sediments – a summary of source, transportation, deposition, and measurement of sediment discharge. *U.S. Geological Survey Bulletin*, 1181-A.

Farrare, H.A., Melfi, S.H., Whiteman, D.N., Evans, K.D., Poellot, H., Kaufman, Y.J. (1998). Raman lidar measurements of aerosol extinction and backscattering 2. Derrivation of aerosol real refractive index, single scattering albedo, and humidification factor using Raman lidar and aircraft size distribution measurements. *Journal of Geophysical Research*, 103, 19 673-19 689.

Gebhart, J. (1992). Performance of a mobile aerosol spectrometer for an in situ characterization on environmental aerosols in Frankfurt City. *Atmospheric Environment*, 26A, 2451-2457.

GRIMM Labortechnik Ltd. (1996). Manual for the Dust Monitor model 1.104 - 1.108 and Software 1.174 (3rd ed.), Germany: GRIMM Labortechnik Ltd.

Gras, J.L., Ayers, G.P. (1983). Marine aerosol at southern mid-latitudes. *Journal of Geophysical Research*, 88 (C15), 10661-10666.

Gunter, Mickey Eugene. (1999). Quartz - the most abundant mineral species in the earth's crust and a human carcinogen? *Journal of Geoscience Education*, 47, 341-349.

Hamonou, E., Chazette, P., Balis, D., Dulac, F., Schneider, X., Galani, E., Ancellet, G., Papayannis, A. (1999). Characterization of the vertical structure of Saharan dust export to the Mediterranean basin. *Journal of Geophysical Research*, 104, 22 257-22 270.

Hidy, G.M. (1975). Summary of the California aerosol characterisation experiment. *Journal of Air Pollution Control Association*, 25, 1106-1114.

Hoek, Gerard, Forsberg, Bertil, Borowska, Margaret, Hlawiczka, Stanislaw, Vaskovi, Eva, Welinder, Hans, Branis, Martin, Benes, Ivan, Kotesovec, Frantisek, Hagen, Leif O., Cyrys, Josef, Jantunen, Matti, Roemer, Willem, Reef, Bert B. (1997). Wintertime PM10 and black smoke concentrations across Europe: results from the Peace Study. *Atmospheric Environment*, 31, 3609-3622.

Hoff, Raymond M., Guise-Bagley, L., Stachler, R.M., Wiebe, H.A., Brook, J. (1996). Lidar, nephelometer, and in situ aerosol experiments in southern Ontario. *Journal of Geophysical Research*, 101, 19 199-19 209.

Hoppel, W.A., Larson, R., Vietti, M.A. (1990). Aerosol size distributions and optical boundaries found in the marine boundary layer over the Atlantic Ocean. *Journal of Geophysical Research*, 95 (D4), 3659-3686.

Hosiokangas, Jari, Ruuskanen, Juhani, Pekkanen, Juha. (1999). Effects of soil episodes and mixed fuel sources on source apportionment of PM10 particles in Kuopio, Finland. *Atmospheric Environment*, 33, 3821-3829.

Keywood, M.D., Ayers, G.P., Gras, J.L., Gillett, R.W., ohen, D.D. (1999). Relationships between size segregated mass concentration data and ultrafine particle number concentrations in urban areas. *Atmospheric Environment*, 33, 2907-2913.

Kleeman, Michael J., Hughes, Lara S., Allen, Jonathan O., Cass, Glen R. (1999). Source contributions to the size and composition distribution of atmospheric particles: southern California in September 1996. *Environmental Science and Technology*, 33(23), 4331-4341.

Kleinman, Lawrence I., Daum, Peter H., Lee, Yin-Nam, Spingston, Stephen R., Newman, Leonard, Leaitch, W. Richard, Banic, Catherine M., Isaac, George A., MacPherson, J.Ian. (1996). Measurement of O_3 and related compounds over southern Nova Scotia. 1. Vertical distribution. *Journal of Geophysical Research*, 101(D22), 29 043-29 060.

Kleinman, Lawrence I., Daum, Peter H., Spingston, Stephen R., Leaitch, W. Richard, Banic, Catherine M., Isaac, George A., Jobson, B. Thomas, Niki, Hiromi. (1996). Measurement of O_3 and related compounds over southern Nova Scotia. 2. Photochemical age and vertical transport *Journal of Geophysical Research*, 101(D22), 29 061-29 074.

Lalas, D.P., Tombrou-Tsella, M., Petrakis, M., Asimakopoulos, D.N., Helmis, C. (1987). An experimental study of the horizontal and vertical distribution of ozone over Athens. *Atmospheric Environment*, 21, 2681-2693.

Le Canut, P., Andreae, M.O., Harris, G.W., Wienhold, F.G., Zenker, T. (1996). Airborne studies of emissions from savanna fires in southern Africa 1. Aerosol emissions measured with a laser optical counter. *Journal of Geophysical Research*, 101 (D19), 23615-23630.

Lehning, M., Richner, H., Kok, G.L., Neininger, B. (1998). Vertical exchange and regional budgets of air pollutants over densely populated areas. *Atmospheric Environment*, 32, 1353-1363.

Lu, R. Turco, R.P. (1994). Air pollutant transport in a coastal environment. Part I. Two-dimensional simulations of sea-breeze and mountain effects. *Journal of the Atmospheric Sciences*, 51, 2285-2308.

Lu, R., Turco, R.P. (1995). Air pollutant transport in a coastal environment. Part II. Three dimensional simulations over Los Angeles Basin. *Atmospheric Environment*, 29, 1499-1518.

Magliano, Karen L., Hughes, Vernon M., Chinkin, Lyle R., Coe, Dana L., Haste, Tami L., Kumar, Naresh, Lurmann, Frederick W. (1999). Spatial and Temporal variations in PM10 and PM2.5 source contributions and comparison to emissions during the 1995 integrated monitoring study. *Atmospheric Environment*, 33, 4757-4773.

McElroy, J.L., Smith, T.B. (1993). Creation and fate of ozone layers aloft in southern California. *Atmospheric Environment*, 27A, 1917-1929.

McKendry, I.G. (2000). PM10 levels in the Lower Fraser Valley, British Columbia, Canada: an overview of spatiotemporal variations and meteorological controls. *Journal of the Air and Waste Management Association*, 50, 443-452.

McKendry, I.G., Lundgren, J. (2000). Tropospheric layering of ozone in regions of urbanized complex and/or coastal terrain: a review. *Progress in Physical Geography*, 24(3), 359-384.

McKendry, I.G., Steyn, D.G., Banta, R.M., Strpp, W., Anlauf, K., Pottier, J. (1998a). Daytime photochemical pollutant transport over a tributary valley lake in Southwestern British Columbia. *Journal of Applied Meteorology*, 37, 393-404.

McKendry, I.G., Steyn, D.G., O'Kane, S., Zawar-Reza, P., Heuff, D. (1998b). Lower tropospheric ozone measurements by light aircraft equipped with chemiluminescent sonde. *Journal of Atmospheric and Oceanic Technology*, 15, 136-143.

McKendry, I.G., Steyn, D.G., Lundgren, J., Hoff, R.M., Strapp, W., Anlauf, K., Froude, F., Martin, J.B., Banta, R.M., Olivier, L.D. (1997). Elevated ozone layers and vertical downmixing over the Lower Fraser Valley, BC. *Atmospheric Environment*, 31, 2135-2146.

Meng, Zhaoyue, Seinfeld, John H., Saxena, Pradeep, Kim, Yong Pyo. (1995). Contribution of water to particulate mass in the South Coast Air Basin. *Aerosol Science and Technology*, 22, 111-123.

Meszaros, A. (1977). On the size distribution of atmospheric aerosol particles and selected combustion sources of indoor particles. *Atmospheric Environment*, 11, 1075-1081.

Morawaska, Lidia, Thomas, Stephen, Jamriska, Milan, Johnson, Graham. (1999). The modality of particle size distributions of environmental aerosols. *Atmospheric Environment*, 33, 4401-4411.

Morawaska, Lidia, Thomas, S., Bofinger, N.D., Wainright, D., Neale, D. (1998). Comprehensive characterisation of aerosols in a subtropical urban atmosphere: particle size distribution and correlation with gaseous pollutants. *Atmospheric Environment*, 32, 2467-2478.

Neu, U., Kunzle, T., Wanner, H. (1994). On the relation between ozone storage in the residual layer and daily variation in the near surface ozone concentration - a case study. *Boundary Layer Meteorology*, 69, 221-247.

Pisano, J.T., McKendry, I.G., Steyn, D.G., Hastie, D.R. (1997). Vertical nitrogen dioxide and ozone concentrations measured from a tethered balloon in the Lower Fraser Valley. *Atmospheric Environment*, 31, 2071-2078.

Porter, J.N., Clarke, A.D. (1997). Aerosol size distribution models based on in situ measurements. *Journal of Geophysical Research*, 102 (D5), 6035-6045.

Pye, Kenneth (ed). (1994). Sediment Transport and Depositional Processes, London: Blackwell Scientific Publications.

Querol, X., Alastuey, A., Puicercus, J.A., Mantilla, E., Miro, J.V., Lopez-Soler, A., Plana, F., Artinano, B. (1998). Seasonal evolution of suspended particles around a large coal-fired power station: particulate levels and sources. *Atmospheric Environment*, 32, 1963-1978.

Raj, P.E., Devara, P.C.S., Maheskumar, R.S., Pandithurai, G. (1997). Lidar measurements of aerosol column content in an urban nocturnal boundary layer. *Atmospheric Research*, 45, 201-216.

Raunemaa, T., Kikas, U., Bernotas, T. (1994). Observation of submicron aerosol black carbon and visibility degradation in remote area at temperature range from -24 to 20°C. *Atmospheric Environment*, 28, 865-871.

Reponen, Auvo, Ruuskanen, Juhani, Mirme, Aadu, Parjala, Erkki, Hoek, Gerard, Roemer, Willem, Hosiokangas, Jari, Pekkanen, Juha, Jantunen, Matti. (1996). Comparison of five methods for measuring particulate matter concentrations in cold winter climate. *Atmospheric Environment*, 22, 3873-3879.

Richards, L. Willard, Alcorn, Siana H., McDade, Charles, Couture, Tiina, Lowenthal, Douglas, Chow, Judith C., Watson, John G. (1999). Optical properties of the San Joaquin Valley aerosol collected during the 1995 integrated monitoring study. *Atmospheric Environment*, 33, 4787-4795.

Serway, Raymond A. (1996). Physics for Scientists and Engineers (4^{th} ed.), Toronto: Saunders College Publishing.

Solomon, Paul A., Magliano, Karen L. (1999). The 1995 Integrated Monitoring Study (IMS95) of the California Regional PM10/PM2.5 Air Quality Study (CRPAQS): a study overview. *Atmospheric Environment*, 33, 4747-4756.

Stettler, M., Hoyningen-Huene, W. (1996). On the relation between haze layer and air mass aerosol at an urban location - case studies. *Atmospheric Research*, 40, 1-18.

Steyn, D.G. (1996). Air pollution in coastal cities. In Gryning, S.E., Schiermeier, F.A., editors. Air Pollution Modelling and its Application XI, New York: Plenum Press.

Steyn, D.G., McKendry, I.G. (1988). Quantitative and qualitative evaluation of the three-dimensional mesoscale numerical model simulation of a sea breeze in comples terrain. *Monthly Weather Review*, 116, 1914-1926.

Strawbridge, K.B., M. Travis and M. Harwood. (2001). Preliminary Results from Scanning Lidar Measurements of Stack Plumes during Winter/Summer. Proceedings of

Laser Radar: Ranging and Atmospheric Lidar Techniques III. Editor: Manfred Ehlers. SPIE Vol. 4546. Toulouse, France. September 2001.

Stull, Roland B. (1988). An Introduction to Boundary Layer Meteorology, Dordrecht: Kluwer Academic Publishers.

Ulrickson, B.L., Mass, C.F. (1990). Numerical investigations of mesoscale circulation over the Los Angeles Basin. Part II. Synoptic influences and pollutant transport. *Monthly Weather Review*, 118, 2162-2184.

Vedal, S. (1997). Ambient particles and health: lines that divide. *Journal of the Air and Waste Management Association*, 47, 551-581.

Wakimoto, R.M., McElroy, J.L. (1986). Lidar observations of elevated pollution layers over Los Angeles. *Journal of Climate and Applied Meteorology*, 25, 1583-1598.

Watson, J.G. (1994). Chemical mass balance source apportionment of PM "sub 10"during the Southern California Air Quality Study. *Aerosol Science and Technology: The Journal of the American Association for Aerosol Research*, 21(1), 1-36.

Zheng, Mei, Fang, Ming, Wang, Fu, To, K.L. (2000). Characterization of the solvent extractable organic compounds in PM2.5 aerosols in Hong Kong. *Atmospheric Environment*, 34, 2691-2702.

Zumdahl, Steven S. (1997). Chemistry (4th ed.), New York: Houghton Mifflin Company.

Appendix I: The GRIMM Particle Dust Monitor Information Sheet

This new state-of-the-art aerosol monitoring system from *GRIMM* is the latest instrument in our renowned line of high speed counters. With a resolution of 1 count/liter, the aerosols are collected on a removable 47 mm Teflon filter for gravimetric or chemical analysis. This unique dual technology is incorporated in all *GRIMM* real-time particle size analyzers. The results can also be analyzed by our 1.174 *GRIMM* Software program and displayed as:

- particle counts in 15 channels
- mass distribution in 15 classes
- environmental PM_{-10}, $PM_{-2.5}$ and PM_{-1}
- occupational as inhalable, thoracic, respirables (alveolics)
- temperature, humidity and wind speed changes

Key Features

Each GRIMM Model 1.108 is hand crafted one at a time to the highest engineering standards and in accordance to the most current ISO 9000 requirements. The Model 1.108 is the only particle size analyzer to offer dual technology consisting of both optical and gravimetrical analysis. Here are some of the additional features:

- Displays real time data in as little as six seconds.
- Portable, weighing only 2.4 kg (5.4 lbs.) with re-chargeable battery.
- 15 different size channels from 0.30 µm to 20 µm
- LCD displays results in particle counts or mass distribution.
- Auto zeros and performs system self-diagnostics at the start of each analysis.
- Removable 47 mm PTFE filter for optional gravimetric and/or chemical analysis of residue.
- Removable data storage cards. Data cards can hold up to one year of data.
- Warning limits can be preprogrammed into the unit with an audible alarm.
- RS 232 serial port for optional computer interface.
- Analog inputs for optional environmental sensors.

Product Specifications

Particle Size	0.30/0.40/0.50/0.65/0.80/1.0/1.6/2.0/3.0/4.0/ 5.0/7.5/10/15/20 µm
Count Range	1 to 100,000 µg/m^3 without any range change
Mass Range	Zero to 100 mg/liter
Sensitivity	1 particle/liter
Sample Flow Rate	1.2 liters/minute, flow controlled
Reproducibility	+/- 2%
Operating Temperature Range	4°C to 45°C

Physical Parameters

Dimensions	24 x 12 x 6cm (9.5 x 5 x 2.5")
Weight	2.4 kg (5.4 lbs.)
Weight Input/Output	lx RS 232, 3x Analog
Power Requirements	Battery or 110/220 VACwith external power supply

The following options and accessories are available:

- Omni-directional, Isokinetic and clean room Sampling Heads
- Stainless Steel or Poly-Resin Housing for outdoor operation
- Temperature, Humidity and Windspeed sensors.
- Carrying case.

Software Options and Data Presentation

The Standard LCD readings are:

- Counts in particles/liter
- Mass as µg/m^3
- Date and Time
- Up to three sensor inputs
- Location
- Battery Status
- Filter Status
- Various system diagnostic and instrument status.

GRIMM's 1.1 74 Software is fully compatible with *WINDOWS* ™95 and 2000. Data can be presented in the following formats:

Environmental Mode: PM_{10}, $PM_{2.5}$ and PM_1 conventions.
Occupational Mode: Inhalable, Thoracic and Respirable (alveolic).
Mass mode: µg/m^3 in 15 size channels
Particle counts: particles/liter in 15 sizes

GRIMM's 1.174 software also offers options for complete statistical analysis of data as well as instrument performance and complete system diagnostics.

Appendix II: Comparison of GRIMM profiles and Lidar images

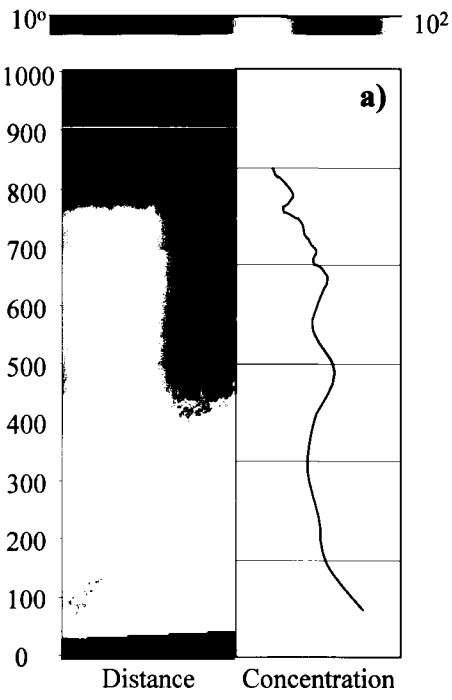

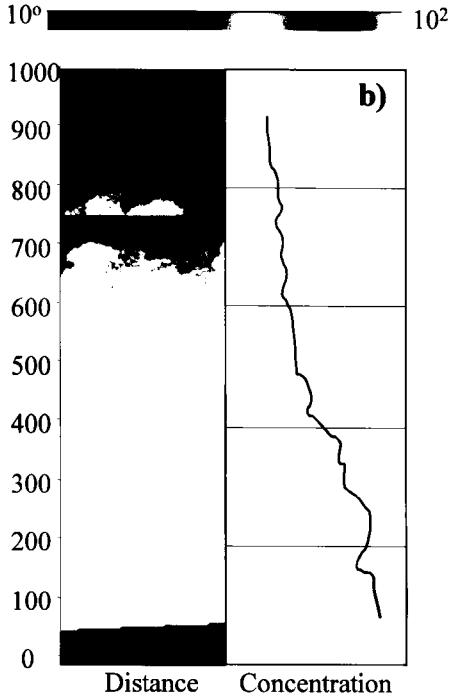

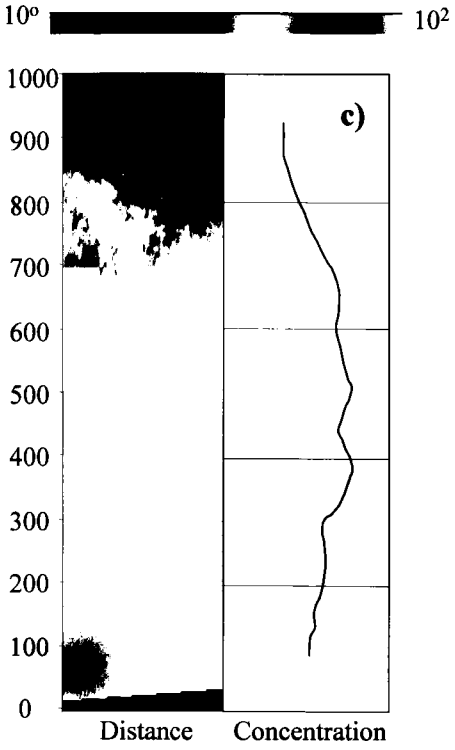

a) **Pitt Meadows: July 26, 2001 09:06 to 09:43**

b) **Pitt Meadows: July 26, 2001 11:01 to 11:45**

c) **Pitt Meadows : July 26, 2001 14:48 to 15:25**

All images have been sliced and Pasted in the vertical to account for the Relatively long time period of each ascent/ Descent sequence.